LegacyClimate 1.0: A dataset of pollen-based climate reconstructions from 2594 Northern Hemisphere sites covering the last 30 ka and beyond

Ulrike Herzschuh[1,2,3], Thomas Böhmer[1], Chenzhi Li[1,2], Manuel Chevalier[4,5], Raphaël Hébert[1], Anne Dallmeyer[6], Xianyong Cao[1,7], Nancy H. Bigelow[8], Larisa Nazarova[1,9], Elena Y. Novenko[10,11], Jungjae Park[12,13], Odile Peyron[14], Natalia A. Rudaya[15,16], Frank Schlütz[17,18], Lyudmila S. Shumilovskikh[18], Pavel E. Tarasov[19], Yongbo Wang[20], Ruilin Wen[21,22], Qinghai Xu[23], Zhuo Zheng[24,25]

[1] Polar Terrestrial Environmental Systems, Alfred Wegener Institute Helmholtz Centre for Polar and Marine Research, Telegrafenberg A45, 14473 Potsdam, Germany

[2] Institute of Environmental Science and Geography, University of Potsdam, Karl-Liebknecht-Str. 24-25, 14476 Potsdam, Germany

[3] Institute of Biochemistry and Biology, University of Potsdam, Karl-Liebknecht-Str. 24-25, 14476 Potsdam, Germany

[4] Institute of Geosciences, Sect. Meteorology, Rheinische Friedrich-Wilhelms-Universität Bonn, Auf dem Hügel 20, 53121 Bonn, Germany

[5] Institute of Earth Surface Dynamics IDYST, Faculté des Géosciences et l'Environnement, University of Lausanne, Bâtiment Géopolis, 1015 Lausanne, Switzerland

[6] Max Planck Institute for Meteorology, Bundesstrasse 53, 20146 Hamburg, Germany

[7] Alpine Paleoecology and Human Adaptation Group (ALPHA), State Key Laboratory of Tibetan Plateau Earth System, and Resources and Environment (TPESRE), Institute of Tibetan Plateau Research, Chinese Academy of Sciences, 100101 Beijing, China

[8] Alaska Quaternary Center, University of Alaska Fairbanks, Fairbanks, Alaska 99775, USA

[9] Kazan Federal University, Kremlyovskaya str. 18, 420008 Kazan, Russia

[10] Lomonosov Moscow State University, Faculty of geography, Leniskie gory 1, 119991 Moscow, Russia

[11] Department of Quaternary Paleogeography, Institute of Geography Russian Academy of Science, Staromonrtny lane, 29, 119017, Moscow, Russia

[12] Department of Geography, Seoul National University, 1 Gwanak-ro, Gwanak-gu, Seoul, 08826, Republic of Korea

[13] Institute for Korean Regional Studies, Seoul National University, 1 Gwanak-ro, Gwanak-gu, Seoul, 08826, Republic of Korea

[14] Institut des Sciences de l'Evolution de Montpellier, Université de Montpellier, CNRS UMR 5554, Montpellier, France

[15] PaleoData Lab, Institute of Archaeology and Ethnography, Siberian Branch, Russian Academy of Sciences, Pr. Akademika 36 Lavrentieva 17, 630090 Novosibirsk, Russia

[16] Biological Institute, Tomsk State University, Pr. Lenina, 26, Tomsk, 634050, Russia

[17] Lower Saxony Institute for Historical Coastal Research, D-26382 Wilhelmshaven, Germany

[18] Department of Palynology and Climate Dynamics, Albrecht-von-Haller Institute for Plant Sciences, University of Göttingen, Untere Karspüle 2, 37073 Göttingen, Germany

[19] Freie Universität Berlin, Institute of Geological Sciences, Palaeontology Section, Malteserstrasse 74-100, Building D, 12249 Berlin, Germany

[20] College of Resource Environment and Tourism, Capital Normal University, 105 West 3rd Ring Rd N, 100048 Beijing, China

[21] Key Laboratory of Cenozoic Geology and Environment, Institute of Geology and Geophysics, Chinese Academy of Sciences, 19 Beitucheng West Road, Chaoyang District, 100029 Beijing, China

[22] CAS Center for Excellence in Life and Paleoenvironment, 100044 Beijing, China

[23] School of Geographic Sciences, Hebei Normal University, 050024 Shijiazhuang, China

[24] Guangdong Key Lab of Geodynamics and Geohazards, School of Earth Sciences and Engineering, Sun Yat-sen University, 519082 Zhuhai, China

[25] Southern Marine Science and Engineering Guangdong Laboratory (Zhuhai), 519082 Zhuhai, China

Correspondence: Ulrike Herzschuh (Ulrike.Herzschuh@awi.de)

Abstract. Here we describe the LegacyClimate 1.0, a dataset of the reconstruction of mean July temperature (T_{July}), mean annual temperature (T_{ann}), and annual precipitation (P_{ann}) from 2594 fossil pollen records from the Northern Hemisphere spanning the entire Holocene with some records reaching back to the Last Glacial. Two reconstruction methods, the Modern Analogue Technique (MAT) and Weighted-Averaging Partial-Least Squares regression (WA-PLS) reveal similar results regarding spatial and temporal patterns. To reduce the impact of precipitation on temperature reconstruction and vice versa, we also provide reconstructions using tailored modern pollen data limiting the range of the corresponding other climate variables. We assess the reliability of the reconstructions using information from the spatial distributions of the root-mean-squared error of prediction and reconstruction significance tests. The dataset is beneficial for synthesis studies of proxy-based reconstructions and to evaluate the output of climate models and thus help to improve the models themselves. We provide our compilation of reconstructed T_{July}, T_{ann}, and P_{ann} as open-access datasets at PANGAEA (https://doi.pangaea.de/10.1594/PANGAEA.930512; Herzschuh et al., 2021). R code for the reconstructions is provided at Zenodo (https://doi.org/10.5281/zenodo.5910989; Herzschuh et al., 2022b), including harmonized open-access modern and fossil datasets used for the reconstructions, so that customized reconstructions can be easily established.

1 Introduction

The comparison of climate model outputs with climate data is essential for model improvements (Eyring et al., 2019). The extratropical Northern Hemisphere is of particular interest because it is known for complex spatial and temporal temperature and precipitation patterns. However, the period for which instrumental observations are available is only of limited use to validate simulations, in particular when assessing climate response to natural climate drivers because it is too short and because it is impacted

by human-induced greenhouse gas forcing. Climate proxy data derived from natural archives are therefore of great value.

Previous proxy-based climate inferences have contributed to major debates about Holocene climate change. For example, while simulations indicate gradual warming of the Holocene, temperature proxy data syntheses rather support a mid-Holocene optimum which resulted in the “Holocene conundrum” debate (Liu et al., 2014). While the debate has progressed since new proxy-based syntheses can help to understand regional differences and contribute further to the debate. Qualitative proxy-based inferences indicate that the mid-Holocene in the Northern Hemisphere mid-latitudes was rather dry and warm compared with present-day in agreement with modeling outputs (Routson et al., 2019). Also, quantitative precipitation reconstructions from Eastern and Central Asia unveiled the complex monsoon-westerlies interactions (Chen et al., 2019; Herzschuh et al., 2019). However, evaluating modeling outputs using proxy-based reconstructions is a complex task and strongly depends on the purpose of the proxy data-model comparison study (e.g. the purpose of an evaluation could either target the mean or site-specific changes, or it could target relative changes or absolute values, or the purpose could be to infer spatial or temporal climate variability at specific scales, etc.). All these types of evaluation require a specific handling of the proxy-data and have to be considered for proxy-model comparisons.

Fossil pollen records are well-established in their use as a palaeoecological and palaeoclimatological proxy and of great value as indicators of past environmental and climatic change for many decades. Considerable efforts have been made to establish regional, continental and even global data repositories like the North American Pollen Database (NAPD; https://www.ncei.noaa.gov/products/paleoclimatology, last access: 1 July 2020), the European Pollen Database (EPD; http://www.europeanpollendatabase.net/index.php, last access: 1 July 2020) and the Neotoma Paleoecology Database (https://www.neotomadb.org/, last access: 1 April 2021; Williams et al., 2018). Pollen data from archives across multiple environmental settings such as lakes, wetlands, or marine sediments, have been widely used to quantitatively reconstruct past vegetation and climate variables (Birks, 2019; Chevalier et al., 2020). Among land-derived proxy data, pollen is particularly suitable for temporarily and spatially high-resolution evaluation of climate model simulations of the late Quaternary period. A number of methods have been proposed for making pollen-based climate reconstructions (Chevalier et al., 2020): among them, classification approaches like the Modern Analogue Technique (MAT) or regression approaches like Weighted-Averaging Partial-Least Squares regression (WA-PLS)

are most commonly used. MAT and WA-PLS rely on extensive collections of modern spectra. Hence, designing a robust calibration dataset from modern pollen assemblages is a crucial part of the reconstruction process. A suitable calibration dataset should cover a wide range of climatic and environmental gradients in order to represent an empirical relationship between pollen assemblages and climate (Birks et al., 2010; Chevalier et al., 2020). Like with fossil pollen records, data syntheses and repositories also exist for modern surface pollen data e.g. for North America (Whitmore et al., 2005), Eurasia (Davis et al., 2013 and 2020) and China (Cao et al., 2013; Herzschuh et al., 2019).

For temperature reconstruction time-series, several broad-scale syntheses exist; however, either they originate from different proxies (Kaufman et al., 2020a and 2020b) or are restricted to certain continents or regions or/and are poorly documented (Mauri et al., 2015; Marsicek et al., 2018; Routson et al., 2019). Temperature reconstructions from extratropical Asia are mostly lacking. Precipitation syntheses are available from Europe (Mauri et al., 2015), North America (Gajewski, 2000) and China and Mongolia (Herzschuh et al., 2019) but, hitherto, no global or hemispheric syntheses of quantitative precipitation changes are available for the Holocene.

In a recent effort, we synthesized and taxonomically harmonized pollen records available in the Neotoma Paleoecology Database (Williams et al., 2018) and additional records from China and Siberia (Cao et al., 2013 and 2020) into a global Late Quaternary fossil pollen dataset (LegacyPollen 1.0; Herzschuh et al., 2022c) and revised all chronologies of those records using a Bayesian approach that allows for the inference of temporal uncertainties (LegacyAge 1.0; Li et al., 2022). Here, in the third part of a series of interconnected studies, we present the pollen-based reconstruction of mean July temperature (T_{July}), mean annual temperature (T_{ann}) and annual precipitation (P_{ann}) including reconstruction and temporal uncertainties as well as quality measures from 2594 records from the Northern Hemisphere using WA-PLS and MAT (LegacyClimate 1.0; this study).

2 Methods

2.1 Input data

The objective of this study is to create a dataset of quantitative reconstructions of T_{July}, T_{ann} and P_{ann} spanning the last 30 ka and beyond from fossil pollen records. These variables (or variables highly correlated to them) were shown to explain most variance in the modern pollen data (T_{July}, P_{ann}) or are

typically used in syntheses and proxy-model comparison studies (T_{ann}). Accordingly, we selected these three variables. We used the fossil data set compiled in LegacyPollen 1.0 (stored on the PANGAEA open data repository and presented in Herzschuh et al., 2022c) that integrates pollen records archived in the Neotoma Paleoecology Database, a dataset from Eastern and Central Asia (Cao et al., 2013; Herzschuh et al., 2019) and a dataset from Northern Asia (Cao et al., 2020). Ages were taken from the "Bacon" (Blaauw and Christen, 2011) age-depth models presented in Li et al. (2022, LegacyAge 1.0), and for each record, we provide an ensemble of 1000 realizations of the age-depth model in our data product so that it can be used to account for chronological uncertainty on the reconstructions. As the chronological and reconstruction errors are independent, they can be added in quadrature to obtain the combined error. With this information, users can easily produce curves with all relevant uncertainties as exemplary shown in Appendix Figure 1.

We compiled the fossil data into four sub-continental datasets for Eastern North America (<104°W; Williams et al., 2000), Western North America, Europe (<43°E) and Asia (>43°E). We restricted the analyses to the 70 most common taxa on each continent to reduce computational power after making sure that higher taxa number would not substantially improve model statistics in climate reconstructions. The number of taxa is limited by the modern training dataset from North America, which contains 70 taxa after applying our taxa harmonization routine (see details in Herzschuh et al., 2022c). We therefore restricted the number of taxa in all fossil datasets to keep the taxa comparable for the reconstructions. To identify the most common taxa we used Hill´s N2 diversity index (i.e., the effective number of occurrences of a species in the dataset; Hill, 1973). For all analyses, square-root percentages were used if not indicated otherwise.

A modern pollen training dataset comprised of 15379 sites includes datasets from Eurasia (EMPD1, Davis et al. 2013; EMPD2, Davis et al. 2020; Herzschuh et al., 2019; Tarasov et al., 2011) and North America (Whitmore et al., 2005). The modern pollen datasets were taxonomically harmonized in accordance with the fossil pollen dataset.

The site-specific T_{ann}, T_{July}, P_{ann} were derived from WorldClim 2 version 2.1 (spatial resolution of 30 seconds (~1 km^2), https://www.worldclim.org; Fick and Hijmans, 2017) by extracting the climate data at the location of the modern sample sites using the *raster* package in R (version 3.5-11, Hijmans et al., 2021; R Core Team, 2020). The WorldClim 2 dataset provides spatially interpolated gridded climate

data aggregated from weather stations as temporal averages between 1970-2000 (Fick and Hijmans, 2017). We used monthly average temperature data to extract the mean T_{July} and the "bioclimatic variables" bio1 (T_{ann}) and bio12 (P_{ann}).

2.2 Reconstruction methods

Our reconstruction approach included MAT (Overpeck et al., 1985) and WA-PLS (ter Braak and Juggins, 1993) by applying the MAT and WAPLS functions from the *rioja* package (version 0.9-21, Juggins, 2019) for R (R Core Team, 2020) on our Northern Hemispheric fossil pollen synthesis. For each fossil location, we calculated the geographic distance between each modern sampling site and the fossil pollen record using the *rdist.earth* function from the *fields* R-package (version 10.3, Nychka et al., 2020) and selected a unique calibration set from modern sites within a 2000 km radius. We fixed the radius to 2000 km instead of 1500 km as suggested from a study in Eastern Asia by Cao et al. (2017), because the modern dataset density is rather low in Northern Asia. For the reconstruction with MAT, we used the original pollen percentages of the selected fossil pollen taxa, looking for 7 analogues between the pollen data and the selected calibration dataset. The dissimilarity between the fossil samples and the modern pollen assemblages was determined by squared-chord distance of the percentage data (Simpson, 2012; Cao et al., 2014).

In addition to the classic WA-PLS reconstruction, we also propose WA-PLS_tailored. This approach addresses the problem that co-variation of climate variables today in space is transferred to the reconstruction even if the past temporal relationship among the climate variables mechanistically differs. In fact, this approach aims to make use of the full climate space covered by the modern pollen samples avoiding those samples in the calibration set that cause spatial covariation. This approach is based on the assumption that several climate variables can be reflected in one and the same pollen assemblage because different plant taxa have different optima in temperature and precipitation ranges and might therefore occur with different co-occurrence and abundance pattern. To reconstruct T_{July} we identified the P_{ann} range reconstructed by WA-PLS and extended it by 25% to both ends of the modern P_{ann} range in order to reduce the influence of P_{ann} on T_{ann} and T_{July} reconstruction due to co-variation. We applied the same method to the reconstruction of P_{ann}. T_{ann} and T_{July} were tailored by P_{ann}; P_{ann} was tailored by T_{July} and, additionally, by T_{ann} (illustrated for an example in Appendix Fig. 2). Reconstruction

uncertainties are provided as root mean square errors (RMSE) derived from the output in the MAT and WAPLS functions. Model errors of WA-PLS and MAT are reported as root mean square error of prediction (RMSEP) derived from leave-one-out cross-validation.

We provide site- or sample-specific measures of quality in addition to the error estimates and model statistics to allow the user to assess the quality of the climate reconstruction dataset. First, we applied a Canonical Correlation Analysis (CCA) to the modern training dataset in order to explore the modern relationship between the pollen spectra and the climate variables and to infer the explained variance in the modern pollen dataset by the target climate variables (ter Braak, 1988) by using the *cca* function in the *vegan* R-package (version 2.5-7, Oksanen et al., 2020). The ratio between constrained (λ_1) and unconstrained (λ_2) explained variance was determined for all modern training datasets used for climate reconstructions. High values of λ_1 vs λ_2 (>= 1) are commonly considered as an indicator to measure how well the target environmental variable is related to the variation in the modern pollen data set (e.g. Juggins, 2013). However, most training data sets encompass multiple environmental variables that are often correlated and additional requirements to such variables would be necessary to explain a significant and independent portion of the variation in the training data set. While a careful design of the training data set can help reduce the effect of correlated environmental gradients, it can never eliminate them completely (Juggins, 2013). To infer the analogue quality as an indicator of no-analogue situations we calculated the minimum dissimilarity (squared chord distance) between modern pollen assemblages and fossil pollen assemblages with probability thresholds of 1% (indicating very good analogs), 2.5% (good analogs) and 5% (poor analogs) using the *minDC* function from the *analogue* R-package (version 0.17-6, Simpson et al., 2021).

A statistical significance test (Telford and Birks, 2011) was applied using the *randomTF* function in the *palaeoSig* R-package (version 2.0-3, Telford, 2019). In this test, the proportion of variance in the fossil pollen data explained by the reconstructed environmental variable is estimated from redundancy analysis (RDA) and tested against a null distribution generated by replacing the modern training dataset with randomly generated surrogate fields. The surrogate fields were simulated to have realistic spatial autocorrelation by fitting variograms to the WorldClim 2 temperature and precipitation data; 1000-member ensembles were simulated for each variable. A reconstruction is considered statistically significant if the reconstructed variable explains more of the variance than 95% of the random reconstructions (Telford and Birks, 2011). The reconstructed climate variables were tested as

introducing the environmental variable as a single variable in a run, as well as with partialling out the explained variance in the pollen data by the respective other variables.

We used Plantaginaceae (mostly representing *Plantago lanceolata*-type in Europe) and *Rumex*-type to assess human influence as an indicator for intense herding (Behre, 1988). In addition, we calculated the correlation between the WA-PLS reconstruction of T_{July}, T_{ann} and P_{ann} and the pollen percentages of Plantaginaceae and *Rumex* for 9000, 3000 and 1000 years BP to assess potential biases in the dataset.

3 Dataset description LegacyClimate 1.0: input data, reconstructions and reconstruction model statistics

LegacyClimate 1.0 provides pollen-based reconstructions and sample-specific reconstruction errors of T_{ann}, T_{July} and P_{ann} for 2594 fossil pollen records (i.e., a total of 146067 single pollen samples) from three reconstruction methods (WA-PLS, WA-PLS_tailored, MAT). Furthermore, we provide the method-specific model metadata and quality measures for each record and each climate variable (Table 1). To ease data handling, the dataset files are separated into Western North America, Eastern North America, Europe and Asia.

249 **Table 1.** Structure and content of the LegacyClimate 1.0 data with details about the information
250 contained in the input datasets, in the climate reconstructions and the reconstruction model statistics.

Datasets	Content
Input datasets	Modern pollen dataset of 15379 sites
	Modern dataset of T_{ann}, T_{July}, P_{ann}
	Fossil pollen data (LegacyPollen 1.0) for 2594 sites with a total of 146067 samples
	Bacon age-depth models (LegacyAge 1.0) for 2579 sites
LegacyClimate 1.0: Climate reconstructions	Reconstructions and sample-specific reconstruction errors of T_{ann}, T_{July} and P_{ann} for 2593 sites using MAT, WA-PLS and WA-PLS_tailored
	Ensemble of 1000 realizations of the Bacon age-depth models for 2579 sites
LegacyClimate 1.0: Reconstruction model statistics	**Site information** (Event label, Source, ID, Site name, Longitude, Latitude)
	Modern pollen dataset information (number of modern analogues, range of climate variables)
	Model statistics for each site for MAT, **WA-PLS, WA-PLS_tailored** (including r^2 observed vs. predicted, RMSEP, no. of WA-PLS components)
LegacyClimate 1.0: Quality Measures	**Canonical Correlation Analysis (CCA)** of the modern training dataset
	Minimum dissimilarities between modern pollen assemblages and fossil pollen assemblages for each record sample for MAT
	Statistical significances sensu Telford & Birks (2011) for each site for MAT, WA-PLS, WA-PLS_tailored

4 Dataset assessment

4.1 Spatial and temporal coverage of LegacyClimate 1.0

In total, we provide reconstructions for 2594 fossil pollen records. Among them 670 records are located in Eastern North America, 361 records in Western North America, 1075 records in Europe and 488 Asian records (Fig. 1). Some few records are included that come from marine cores which were taken from the continental shelf. They contain information from source areas from the nearby continents (e.g. fluvially transported material). If users want to focus on terrestrial-only records, those marine sites could be filtered out by the archive type provided in the metadata. Climate reconstructions for one fossil record in the Western North American Dataset on Hawaii (Dataset-ID 17832, “Kealia Pond”) could not be performed as there were no modern training data available within a 2000 km area.

The temporal coverage of the records is rather uneven: 75 and 666 records cover the periods between 30-29 ka and 15-14 ka, respectively (Fig. 2).

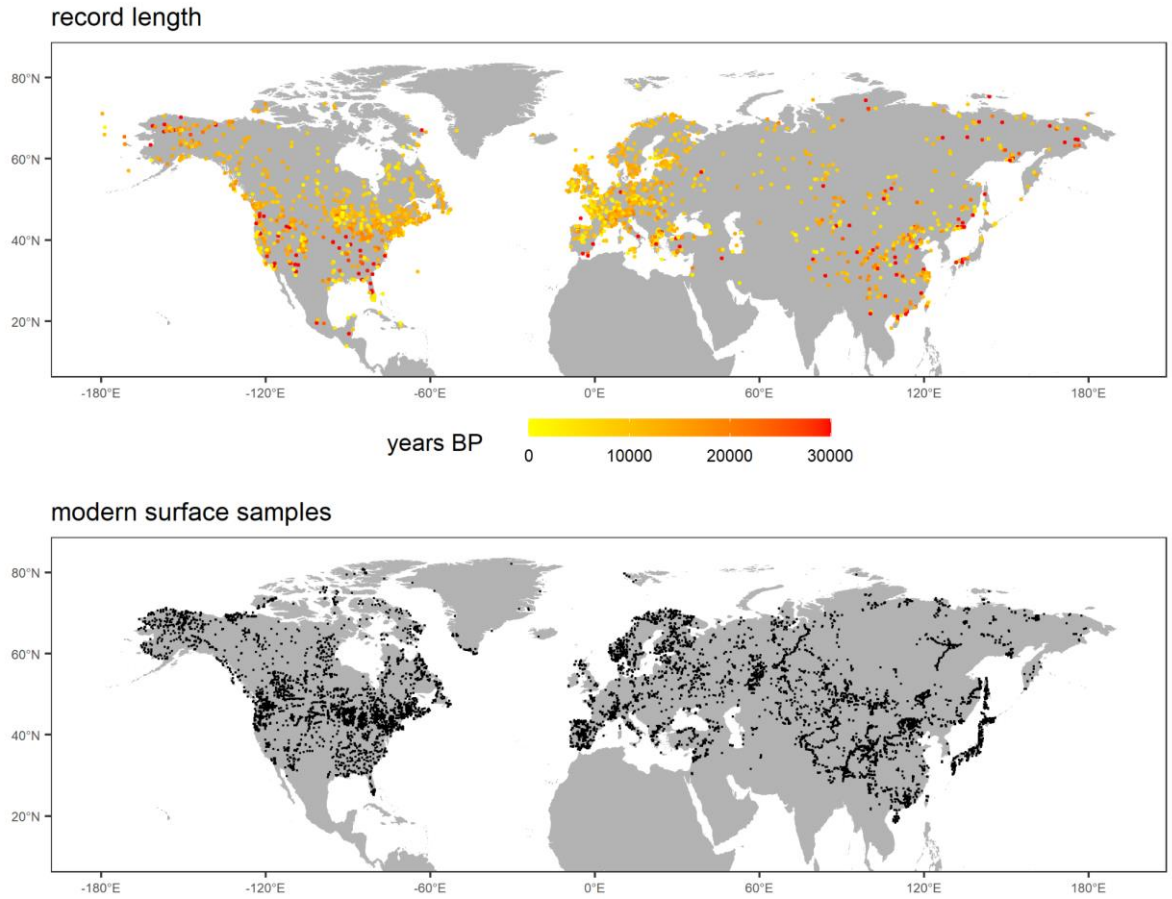

Figure 1. Upper panel: map indicating the spatial distribution and record lengths covered by the LegacyPollen 1.0 dataset (Herzschuh et al., 2022c) for which climate reconstructions, temporal and reconstruction uncertainties and reconstruction quality measures are provided in LegacyClimate 1.0 with a total of 2594 records; Lower panel: spatial distribution of modern pollen dataset used for reconstruction with a total of 15379 sites.

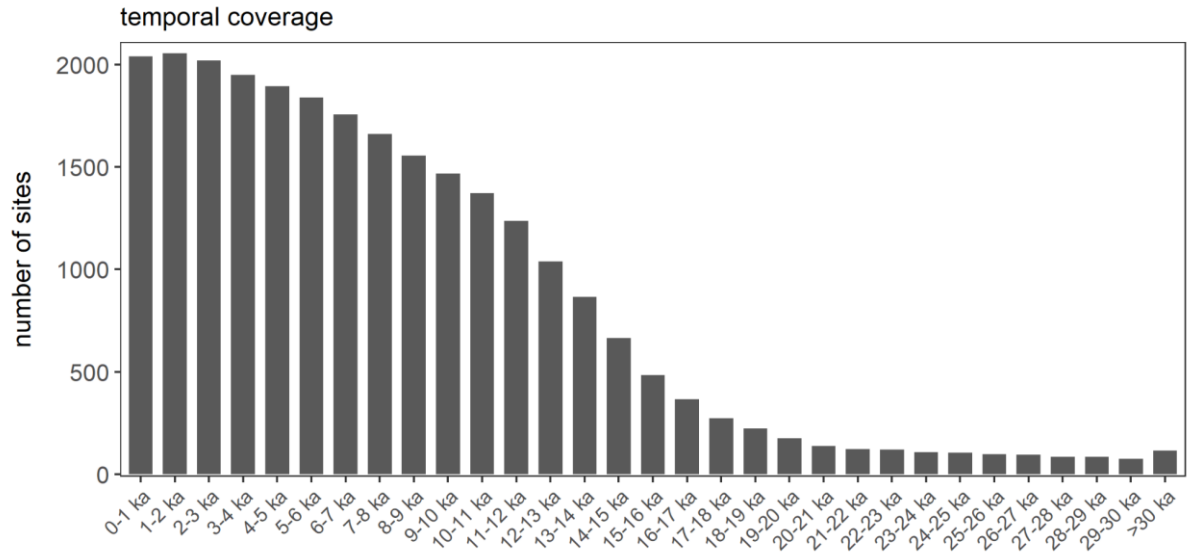

Figure 2. Number of records that cover certain millennia of the last 30 ka.

4.2 Modern relationships between pollen and climate assessed by constrained ordination.

Results from CCA applied to modern datasets reveal that T_{July}-constrained ordinations have high λ_1/λ_2 ratios, indicating a strong relationship between this climate variable and modern pollen assemblages, in Eastern North America while low ratios can be found in Central Asia. The spatial pattern of λ_1/λ_2 of ordinations constrained by T_{ann} is overall similar to those of T_{July} but the ratios are slightly higher for T_{ann} than for T_{July}. Reconstructions for P_{ann} show low ratios in Europe and Eastern North America. Areas with high ratios are concentrated in Alaska and East Asia (Fig. 3).

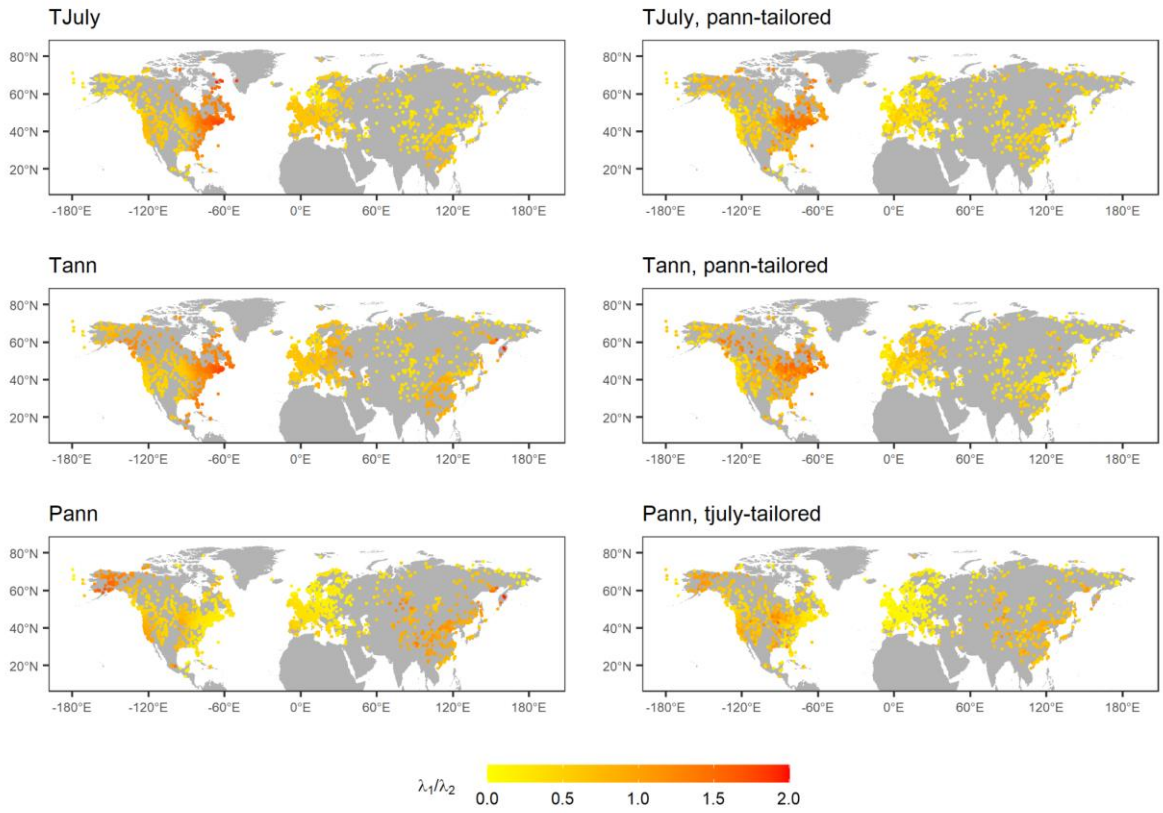

Figure 3. Maps showing λ_1/λ_2, representing the ratio of explained variance of first axis (constrained) vs. second (unconstrained) axis as revealed by applying a CCA to all modern training datasets that were used for the reconstructions. High ratios (>=1) indicate a strong relationship between the modern pollen datasets and climate and can be used to determine ecologically important determinants. Constraining variables as well as tailoring of the dataset (see methods) is indicated in the map captions.

4.3 Analogue quality

The dissimilarity (squared chord distance) between modern pollen assemblages and fossil pollen assemblages was calculated and extracted for distinct time-slices at 9000, 6000 and 3000 years BP. In total, 36.4% (9000 years BP), 39.2% (6000 years BP) and 45.6% (3000 years BP) records indicate a very good (<1%) analogue quality. The central part of the North American continent, Scandinavia and Central Asia show a very good analogue quality for all time-slices investigated. Poor (<5%) analogues can be found in Western Europe, the eastern parts of the United States and along the eastern Asian coastline. Non-analogues (>5%) are found for 22.6% (9000 years BP), 20.47% (6000 years BP) and 12.5% (3000 years BP) record respectively, especially in Western Europe and at 9000 years BP in Alaska (Fig. 4).

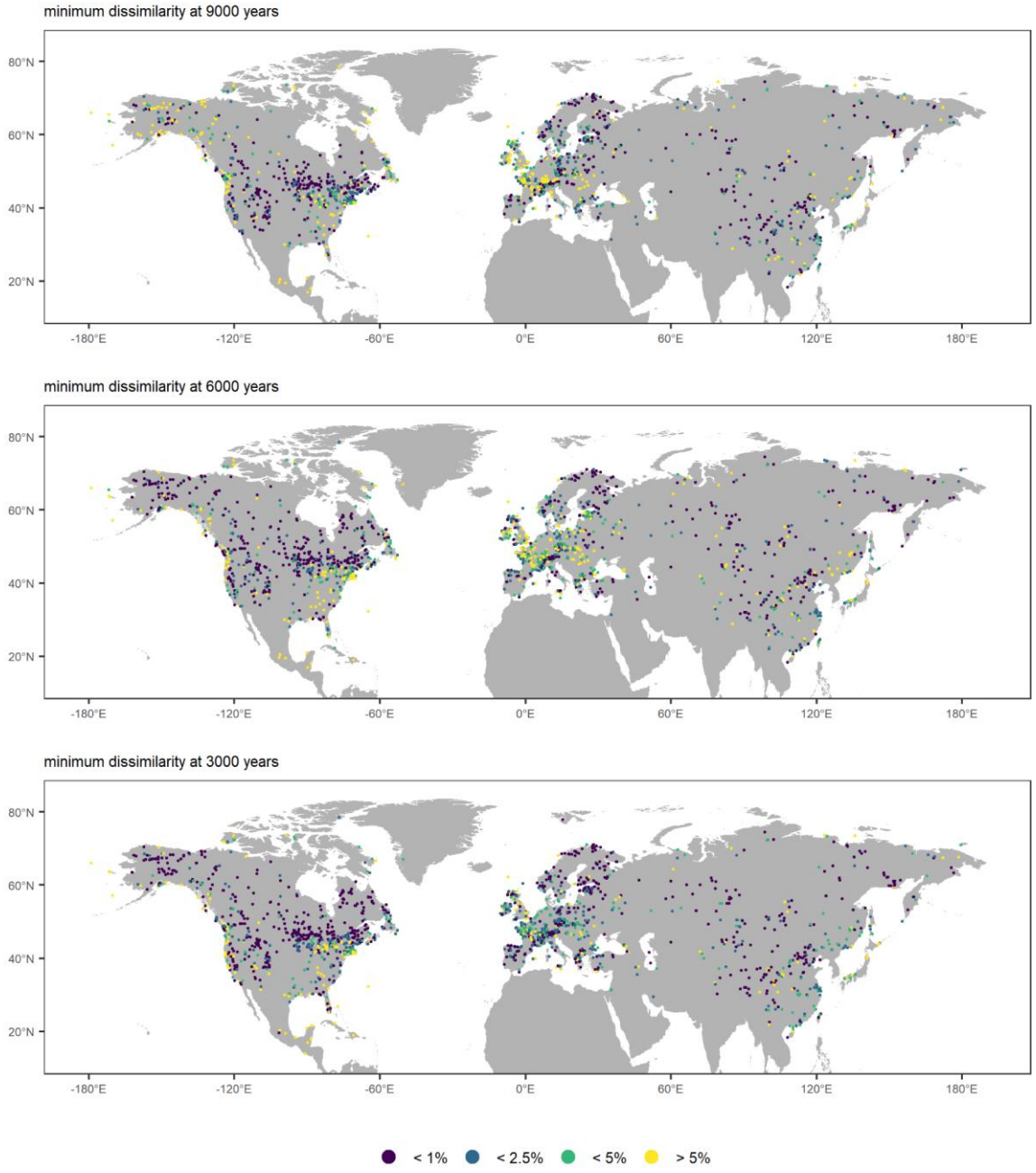

Figure 4. Analogue quality as assessed by squared chord distance between modern pollen assemblages and fossil pollen assemblages. Results identify very good (<1%), good (<2.5%) and poor (<5%) analogues. Distances >5% are considered to indicate non-analogue situations (as percentage of all distances among pollen samples in the modern dataset used for calibration).

4.4 Prediction errors of LegacyClimate 1.0

The mean RMSEPs and their standard deviations for T_{ann} are 1.98±0.52°C (MAT), 2.61±0.53°C (WA-PLS) and 2.24±0.61°C (WA-PLS_tailored) and mean RMSEPs as a percentage of modern T_{ann} range are 7.68±1.93% (MAT), 10.09±2.05% (WA-PLS) and 10.26±2.79% (WA-PLS_tailored). The largest mean RMSEP values are located in Central Asia in Kazakhstan, Mongolia and the north-western parts of the Tibetan Plateau and are consistent across all three reconstruction methods. Other areas with large mean RMSEP values are located in Western North America, Southern and Central Europe and south-east Asia. The smallest RMSEPs can be found along the east coast of North America. Relative to the modern temperature range, the RMSEP from this region also reveals the lowest fraction. In general, MAT has the lowest mean error fraction relative to the modern temperature range of all three methods.

The mean RMSEPs of T_{July} are 1.90±0.63°C (MAT), 2.50±0.73°C (WA-PLS) and 2.21±0.75°C (WA-PLS_tailored) and mean percentages of T_{July} range are 8.11±1.64% (MAT), 10.71±1.94% (WA-PLS) and 10.70±2.60% (WA-PLS_tailored). Thus, they are slightly smaller than those of T_{ann} but slightly larger as a percentage of the range. The spatial patterns, however, are largely similar to those of T_{ann}.

The mean RMSEPs of P_{ann} are 176.38±51.40 mm (MAT), 244.48±75.84 mm (WA-PLS) and 232.71±98.57 mm (WA-PLS_tailored) and mean percentages of P_{ann} range are 6.78±1.48% (MAT), 9.27±1.70% (WA-PLS) and 10.26±2.67% (WA-PLS_tailored). High RMSEPs are found for Western North America, Europe and along the coastline of south-east Asia, while the lowest RMSEP values are found for Central Asia. A clear division in RMSEPs are found on the North American continent: while the western part of North America (with the exception of Alaska) has a rather high RMSEP, the eastern part of North America has a smaller RMSEP. This pattern is found for all three methods (Fig. 5).

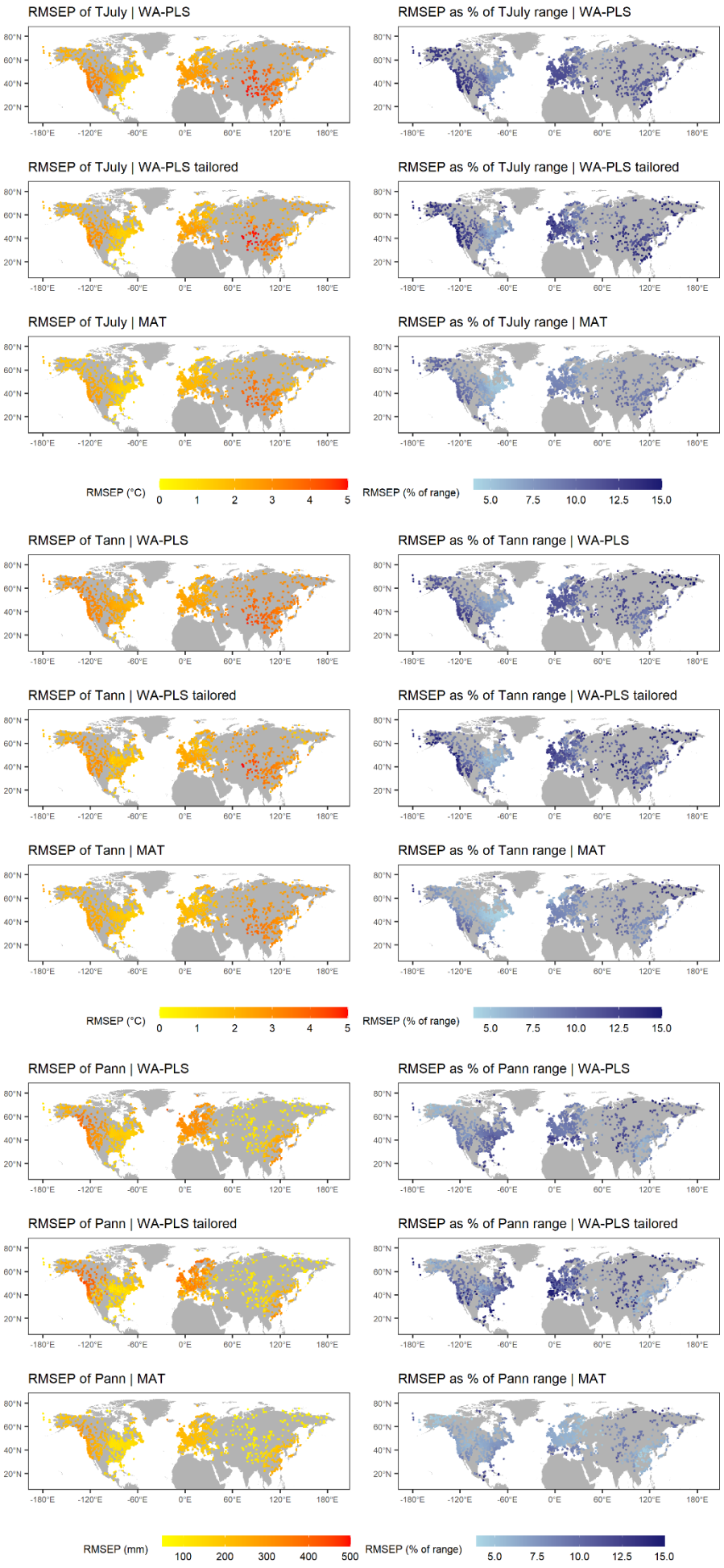
RMSEP of TJuly | WA-PLS
RMSEP as % of TJuly range | WA-PLS
RMSEP of TJuly | WA-PLS tailored
RMSEP as % of TJuly range | WA-PLS tailored
RMSEP of TJuly | MAT
RMSEP as % of TJuly range | MAT
RMSEP (°C) 0 1 2 3 4 5
RMSEP (% of range) 5.0 7.5 10.0 12.5 15.0
RMSEP of Tann | WA-PLS
RMSEP as % of Tann range | WA-PLS
RMSEP of Tann | WA-PLS tailored
RMSEP as % of Tann range | WA-PLS tailored
RMSEP of Tann | MAT
RMSEP as % of Tann range | MAT
RMSEP (°C) 0 1 2 3 4 5
RMSEP (% of range) 5.0 7.5 10.0 12.5 15.0
RMSEP of Pann | WA-PLS
RMSEP as % of Pann range | WA-PLS
RMSEP of Pann | WA-PLS tailored
RMSEP as % of Pann range | WA-PLS tailored
RMSEP of Pann | MAT
RMSEP as % of Pann range | MAT
RMSEP (mm) 100 200 300 400 500
RMSEP (% of range) 5.0 7.5 10.0 12.5 15.0

Figure 5. Spatial distribution of root-mean-squared error of prediction (RMSEP) as inferred from leave-one-out cross-validation presented as absolute values and as a percentage of the range of mean July temperature (T_{July}), mean annual temperature (T_{ann}), annual precipitation (P_{ann}) in the modern pollen data used for reconstruction for the three methods applied (Weighted-Averaging Partial-Least Squares regression (WA-PLS), WA-PLS using a training set from within a limited climate range (WA-PLS_tailored) and Modern Analogue Technique (MAT)).

4.5 Significance test

A significance test ($p < 0.1$ and in addition $p < 0.2$, see methods) according to Telford and Birks (2011) was performed for each record (Fig. 6; Table 2). For the T_{July} reconstruction, 16.4% [p<0.2: 27.2%] (WA-PLS) and 19.0% [p<0.2: 29.1%] (WA-PLS_tailored) of all records passed the significance test when included as a single variable in the significance test. Partialling out precipitation as a conditional variable causes an increase in the amount of significant records to 19.0% [p<0.2: 30.6%] for WA-PLS of T_{July}, but a decrease for WA-PLS_tailored to 16.7% [p<0.2: 27.6%] of all records. The T_{ann} reconstruction is significant for 16.5% [p<0.2: 27.1%] (WA-PLS) and 20.0% [p<0.2: 31.6%] (WA-PLS_tailored) of all records when tested as a single variable. When partialling out precipitation, the amount of significant records slightly increases for WA-PLS, but decreases for WA-PLS_tailored. 13.0% [p<0.2: 21.8%] (WA-PLS) and 14.3% [p<0.2: 25.4%] (WA-PLS_tailored) of all records pass the significance test when testing P_{ann} as a single variable. Partialling out the mean July temperature as a conditional variable increases the number of significant records for both WA-PLS and WA-PLS_tailored.

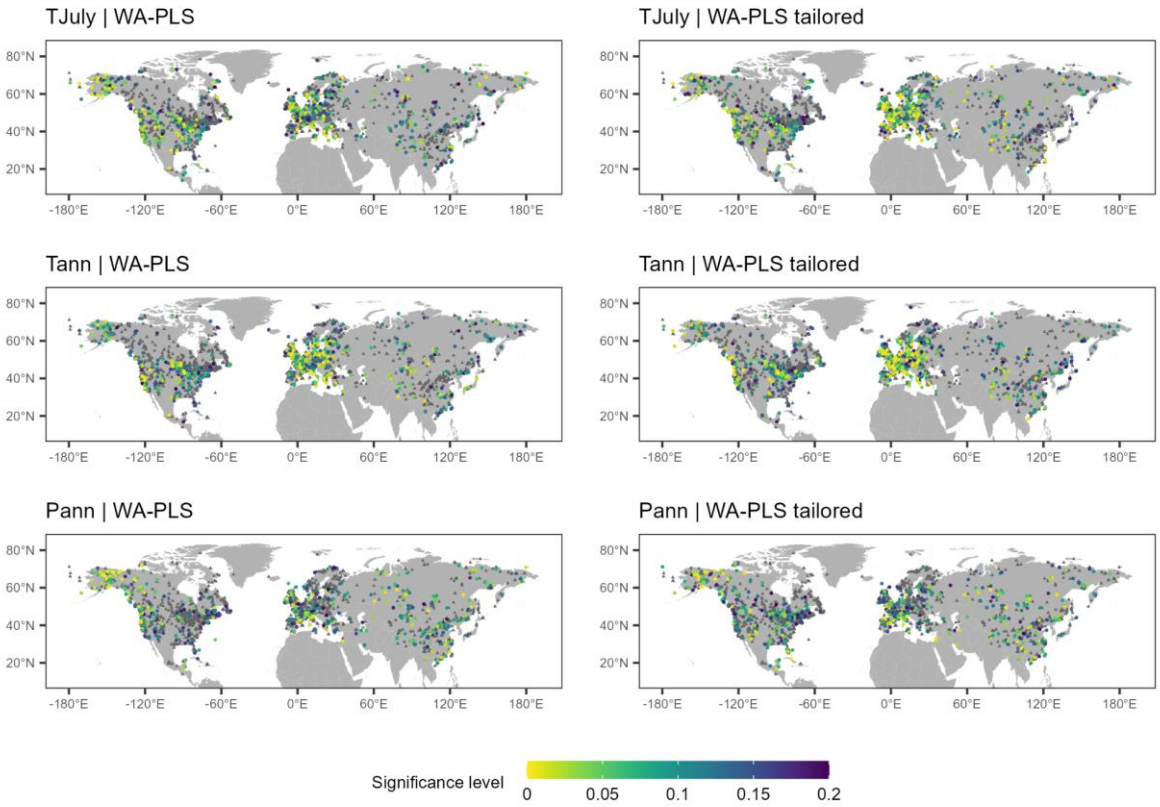

348

349 **Figure 6.** Maps showing mean July temperature (T_{July}), mean annual temperature (T_{ann}), annual
350 precipitation (P_{ann}) records that passed the reconstruction significance test ($p<0.2$). Colors indicate the
351 significance level. Records that did not pass the significance level ($p>=0.2$) are shown as grey
352 rectangles.

353

354

355

356

357

358

359

360

361

362 **Table 2.** Percentage of records that pass the reconstruction significance test (p<0.1 and p<0.2) sensu
363 Telford and Birks (2011). The values in brackets for p<0.1 indicate the significance values without taking
364 spatial autocorrelation into account.

	WA-PLS		WA-PLS_tailored		MAT	
	p < 0.1	p < 0.2	p < 0.1	p < 0.2	p < 0.1	p < 0.2
T_{July}	16.4% (30.9%)	27.2%	19.0% (35.2%)	29.1%	44.1% (42.4%)	56.8%
T_{July} partialling out P_{ann}	19.0% (35.5%)	30.6%	16.7% (33.6%)	27.6%	48.7% (39.9%)	61.4%
T_{ann}	16.5% (32.8%)	27.1%	20.0% (36.1%)	31.6%	46.5% (42.4%)	57.7%
T_{ann} partialling out P_{ann}	16.7% (32.6%)	27.1%	18.4% (34.1%)	28.8%	48.1% (39.2%)	61.9%
P_{ann}	13.0% (32.1%)	21.8%	14.3% (33.4%)	25.4%	36.5% (36.3%)	51.1%
P_{ann} partialling out T_{July}	14.5% (34.2%)	24.1%	16.5% (36.5%)	28.2%	39.4% (34.5%)	53.7%

365

366

367

368 **4.6 Human impact**

369 We used the abundance of Plantaginaceae and *Rumex* as indicators of grazing and such intense animal
370 husbandry. Overall weak human impact is inferred for North America and Northern Asia. The indicators
371 show strong human impact only in individual records at 9000 years BP in China and the Mediterranean
372 region (Fig. 7). The percentage values of Plantaginaceae and *Rumex* were high especially in Europe
373 for 3000 years and 1000 years BP which indicates growing human impact on that region. High
374 Plantaginaceae correlate with low T_{July} and high P_{ann} in Central Europe indicating potential biases in the
375 temperature reconstructions i.e. too low temperatures become reconstructed. Similar correlations are
376 found for Rumex, especially in Northern Europe (Fig. 8).

377

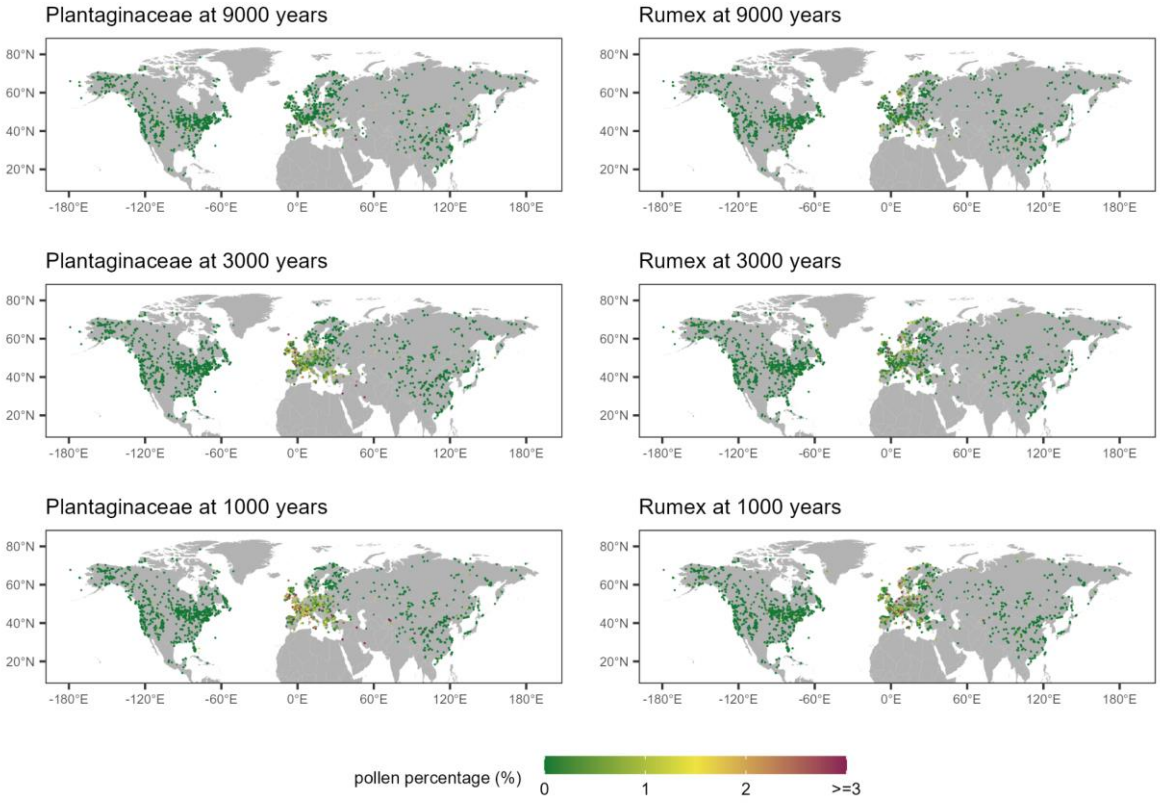

378

379 **Figure 7.** Abundance of Plantaginaceae (left) and *Rumex* (right) at 9000, 3000 and 1000 years BP.
380 Colors indicate percentage values.

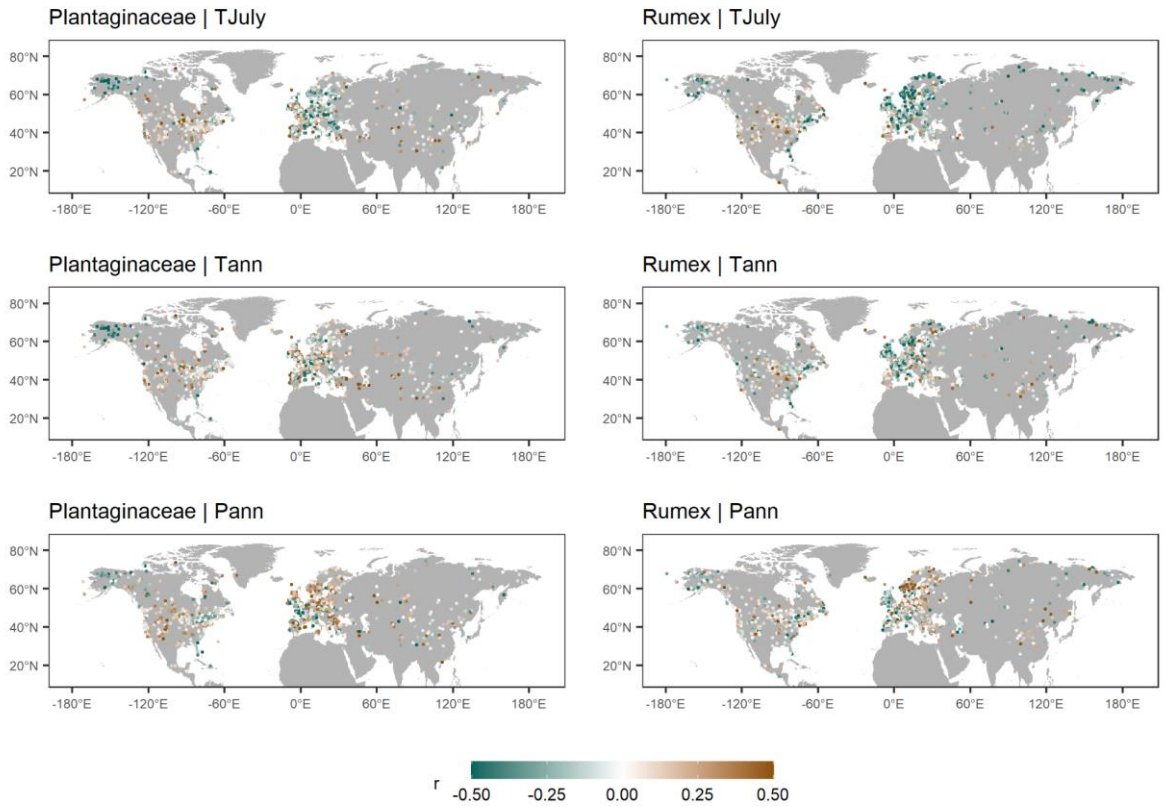

Figure 8. Correlation between the percentage of Plantaginaceae (left) and *Rumex* (right) and reconstructed T_{July}, T_{ann} and P_{ann} with WA-PLS.

4.7 Assessment of major temporal patterns of LegacyClimate 1.0

To illustrate the difference between Mid- and Late Holocene climate, we calculated the value for the three climate variables at 6 ka BP and 1 ka BP, each time taking the average of the interpolated values at those ages for the ensemble of 1000 realizations of the age-depth models (Li et al., 2022). Differences between these time-slices reveal warmer and drier conditions during the Mid-Holocene compared with Late Holocene conditions, especially in Eastern North America, but also in Central and Northern Europe. The overall patterns are in good agreement for all three methods but show differences on a regional scale, especially when comparing the reconstructions with WA-PLS and MAT. For T_{July}, the reconstruction with MAT shows greater temperature differences in Western North America and south-east Asia. Compared to the reconstruction with WA-PLS, there is a reduced cooling from 6 ka to 1 ka in Eastern Europe and a warming instead of a cooling in the Western Mediterranean region and along the south-eastern Asian coastline in MAT. For large areas in North America and Europe, the reconstructions with WA-PLS suggest an increase in precipitation from 6 to 1 ka BP. A shift to drier conditions can be

398 found along the south-eastern coastline in North America, in the Mediterranean Region and especially
399 in south-east Asia. The reconstruction with MAT reveals a gradient from increasing precipitation in
400 south-western Europe to decreasing precipitation in north-eastern Europe. In contrast to the
401 reconstructions with WA-PLS, records along the south-eastern Asian coastline suggest an increase in
402 precipitation with MAT rather than a decrease (Fig. 9).

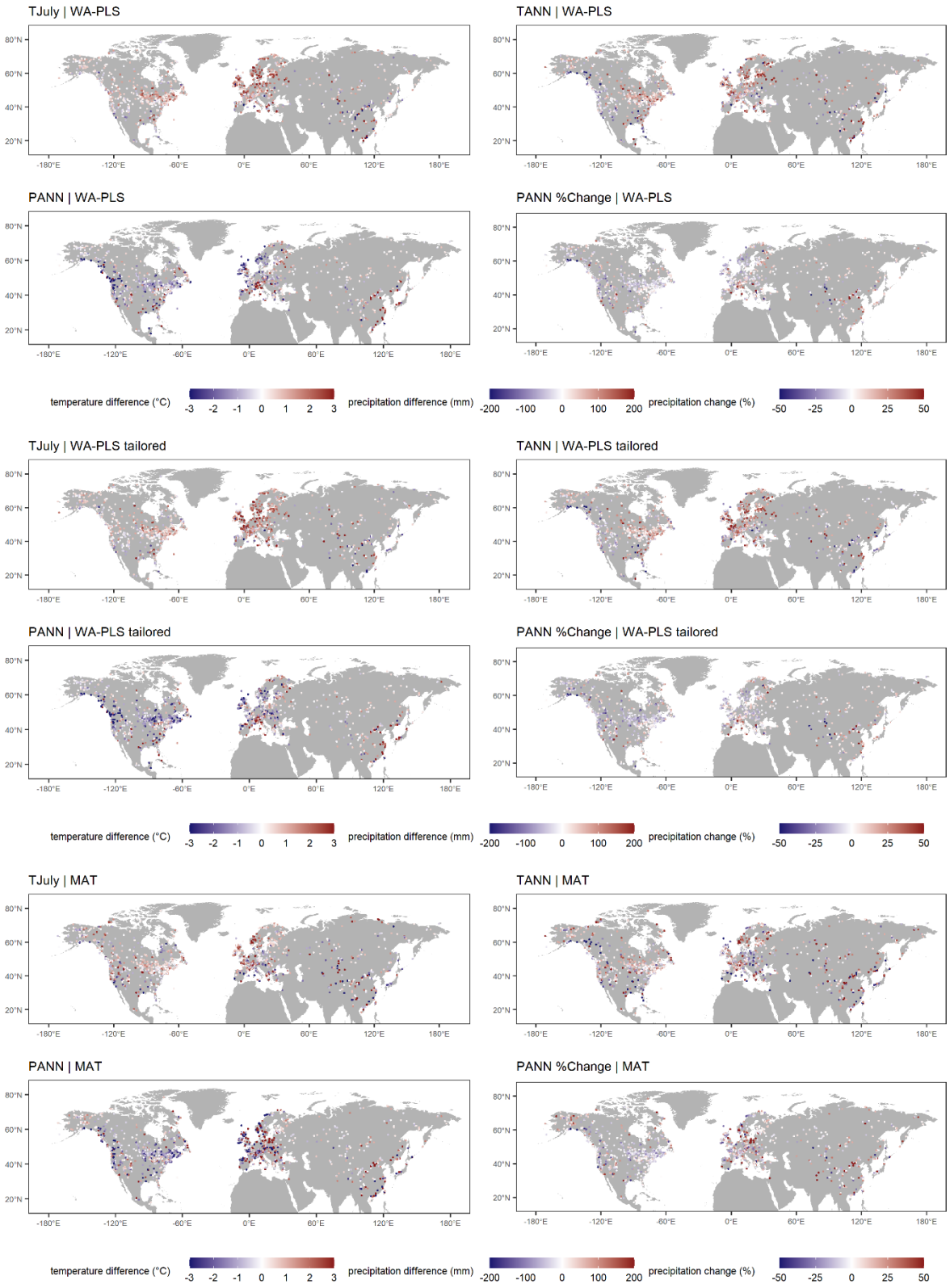

403

404 **Figure 9.** Difference from 6 ka to 1 ka for mean July temperature (T_{July}), mean annual temperature (T_{ann}),
405 annual precipitation (P_{ann}) and P_{ann}% as reconstructed from WA-PLS (upper panel), WA-PLS_tailored
406 (middle panel) and MAT (lower panel).

Time-series of absolute T_{ann} reconstructions reveal temporal as well as latitudinal spatial variation on the single continents. Eastern North America and Asia show the most variation in the low latitudes. It is also Eastern North America which shows the most pronounced latitudinal gradient. In Western North America, the most variation takes place in the high latitudes, while the variation is concentrated to the mid-latitudes in Europe. Especially in North America, the warming since the last deglaciation and the beginning of the Holocene is well shown in the temporal variation of the time-series (Fig. 10).

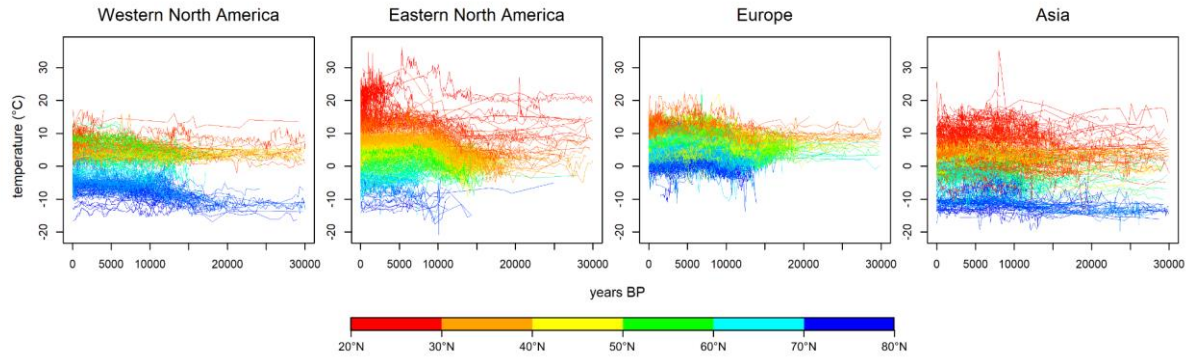

Figure 10. Time-series of absolute mean annual temperature (T_{ann}) reconstruction with WA-PLS for each (sub-)continent. Colors denote the latitude of record origin. Age and reconstruction uncertainties are not plotted but are available for each time-series.

4.8 Assessment of consistency among reconstruction methods

Reconstructions with MAT are, in general, in good agreement with those derived from the WA-PLS. Comparing MAT with WA-PLS, 37.3% (T_{July}), 38.9% (T_{ann}) and 30.4% (P_{ann}) of all records have a positive correlation of r >= 0.6. Strong positive correlations (r >= 0.9) can mainly be identified in Eastern North America, while weak correlation can be found for large areas in central North America and most of Europe (Fig. 11).

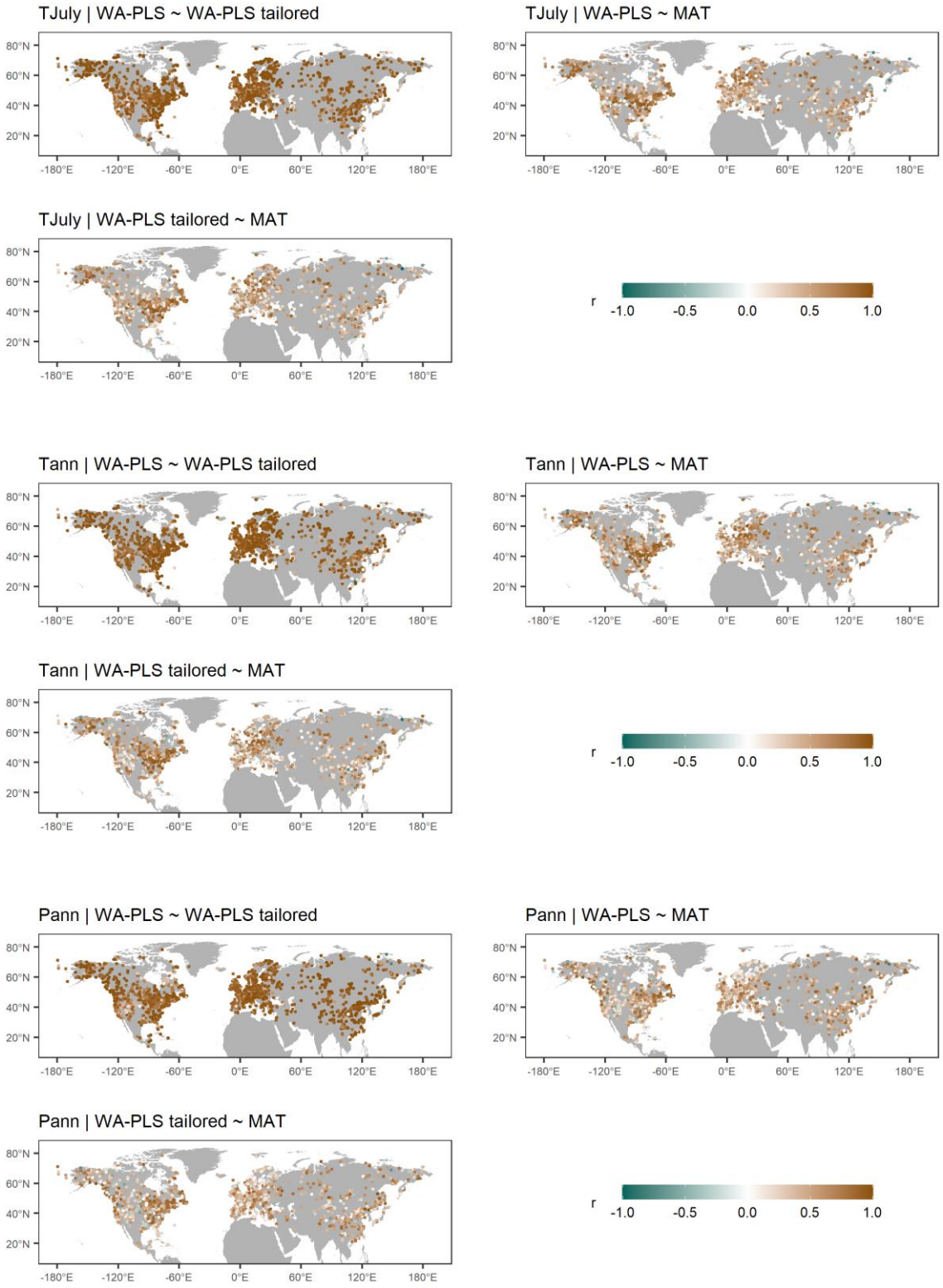

425

426 **Figure 11.** Correlation between time-series of the 3 different reconstruction methods used - weighted-
427 averaging partial least squares using a global training set (WA-PLS), WA-PLS using a training set with
428 a limited modern climate range (WA-PLS_tailored) and the modern analogue technique (MAT) for the

three climate variables of mean July temperature (T_{July}), mean annual temperature (T_{ann}) and annual precipitation (P_{ann}).

WA-PLS_tailored used a reduced modern training dataset (illustrated for an example in Appendix Fig. 2). The tailoring successfully reduced the co-variation of temperature and precipitation in the modern dataset as indicated by the distribution of the correlation coefficient in Fig. 12. Nevertheless, the obtained reconstructions are largely consistent between WA-PLS and WA-PLS-tailored: a correlation of r >= 0.9 is found for 59.2% of all records for T_{July}, 60.7% for T_{ann} and 56.5% for P_{ann}.

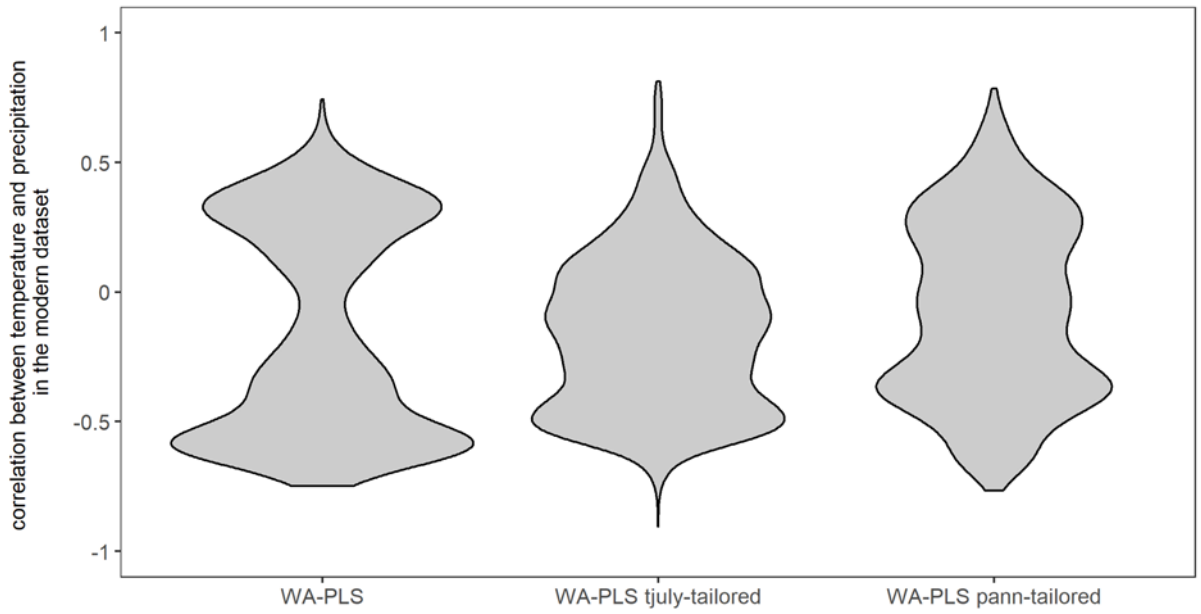

Figure 12. Violin plot of the correlation coefficients between T_{July} and P_{ann} in the 15379 training datasets used for the reconstructions. Left: used for WA-PLS reconstructions; middle: WA-PLS T_{July}-tailored (used for the reconstruction of P_{ann}); WA-PLS P_{ann}-tailored (used for the reconstruction of T_{July}).

5 Discussion

5.1 Impact of the fossil pollen data source on LegacyClimate 1.0 quality

LegacyClimate 1.0 contains reconstructions of climate variables from fossil pollen data derived from open-access data repositories. The fossil records were derived from multiple natural archives, most commonly, assemblages from continuous lacustrine and peat accumulations (Herzschuh et al., 2022c).

Different sizes of lakes and peat areas result in varying sizes of pollen source areas and thus the spatial representativeness of a record. While small lakes and peatlands are considered to provide information about the (extra-)local scale, the regional signal is better represented in pollen assemblages from large lakes (Jackson, 1990; Sugita, 1993). However, taphonomic changes of the records originating, for example, from lake level changes may impact the reconstructed climate. Pollen from azonal riverine vegetation might be over-represented in fluvially impacted pollen records.

Our dataset is based on taxonomically harmonized modern and fossil pollen datasets using a restricted number of taxa. Such an approach guarantees that all records are handled consistently. Although losing taxonomic information when merging taxa together into a higher taxonomic level, it also increases the possibility of matching climate analogues in the modern and the fossil datasets. However, one needs to keep in mind that species with different ecological requirements may be merged together into one genus or family, for example, *Pinus* species that are restricted to tropical or subtropical areas in China or ones that grow in boreal forests (Cao et al., 2013; Tian et al., 2017).

Along with the pollen assemblages, data repositories also provide chronological information for fossil records. The quality of such chronologies varies strongly with respect to dating methods, calibration and numerical algorithms for determining an age-depth relationship (Blois et al., 2011; Trachsel and Telford, 2017). Having accurate and precise chronologies is thus of pivotal importance for reconstructing past climate in order to identify temporo-spatial patterns and therefore in helping to evaluate climate model outputs. The advantage of the fossil pollen dataset used for the reconstruction presented here (i.e., LegacyPollen 1.0; Herzschuh et al., 2022c) is that it has harmonized chronologies (LegacyAge 1.0) along with information about uncertainties as well as related metadata and scripts that allow a customized re-establishment of the chronologies (Li et al., 2022). Accordingly, we were able to provide sample specific age-uncertainties along with reconstruction uncertainties.

5.2 Modern pollen and climate data sources and LegacyClimate 1.0 quality

We a priori selected T_{July}, T_{ann} and P_{ann} as target variables for our reconstructions. However, we provide λ_1/λ_2 (i.e. explained variance of the climate variable in the modern pollen data set relative to the variance explained by the unconstrained first axis; ter Braak, 1988), a commonly used proxy for the assessment of reconstructions. The higher λ_1/λ_2 in the spatial modern dataset the higher the chance that this target

climate variable has also impacted vegetation over time and is thus reflected in the variation of the fossil pollen dataset. As a rule of thumb, a ratio of 1 is considered to indicate reliable reconstructions (Juggins, 2013) though useful reconstructions may also be obtained from datasets with lower values. As expected, maps of RMSEPs reveal similar spatial pattern as the results of constrained ordination. Our results indicate that in particular calibration sets from Europe have low ratios and a high RMSEP for all climate variables (despite having a high number of modern samples), likely related to the human impact on the modern and fossil data. Some areas that are known for its sensitivity to precipitation e.g. Eastern Asia show low RMSEPs as expected for P_{ann} but on the other hand show a low sensitivity to T_{ann} and T_{July}.

For our study we used the, to our knowledge, largest modern dataset ever used in a pollen-based climate reconstruction. For fossil pollen records in areas with an insufficient coverage of modern surface pollen samples (e.g., Central Asia or Western Siberia), it might be difficult to create a calibration dataset that maps the required variety of environmental and climatic gradients and therefore find enough modern analogues for reconstructions with a classification approach such as MAT. This is indicated by the high RMSEPs as percentages of gradient length in these areas. Our routine uses the modern pollen data from within a radius of 2000 km around the site of the fossil record. The information provided in the reconstruction metadata including number of modern pollen samples and ranges of reconstructed variables, allow an assessment of the modern dataset used for reconstruction. Our assessments of the modern dataset (e.g. using CCA), the transfer function (e.g. RMSEP) and the reconstruction (e.g. the significance test) revealed also the potential biases in the pollen-based reconstruction and pointed to limitations. Further validation and assessments of the results and more comprehensive uncertainty analyses e.g. by applying forward modelling approaches (Izumi & Bartlein, 2016; Parnell et al., 2016) would be highly valuable.

5.3 Reconstruction method and LegacyClimate 1.0 quality

Overall, the three reconstruction approaches, MAT, WA-PLS and WA-PLS_tailored yield rather similar results i.e. indicated by the overall high correlation between the reconstructions of the different methods (Fig. 11). Accordingly, the major trends at global or continental scales are similar, even if the actual amplitude of change may vary locally. As each method has its own strengths and weaknesses, there is not one set of reconstructions that is absolutely superior. One advantage of our multi-method reconstruction dataset is that users can identify the methods that are likely to perform best in a selected

region and/or specific reconstructions. MAT is often recommended for large-scale studies, but it is highly sensitive to the quality of analogues (Chevalier et al. 2020). Low analogue situations can arise from two causes: climate conditions that differ strongly from today (e.g., the low atmospheric CO_2 concentration during the LGM; Jackson and Williams, 2004), or in regions with limited modern samples (e.g., extratropical Asia). Furthermore, growing human influence on the landscape since the Middle to Late Holocene especially in densely settled regions in Europe contributed to gaps within the potential bioclimatic space of taxa and probably also led to extinction events, especially for disturbance-dependent taxa (Zanon et al., 2018). We report the analogue distance for each sample to help identify such situations. From our assessments, we revealed that analogues quality is overall rather good at least for the Holocene and except for Western Europe in particularly the British Isles (Fig. 4).

In contrast to MAT, WA-PLS (and most regression techniques in general) model relationships between pollen and climate and are, as such, less sensitive to the low analogue situations (Birks et al., 2010). They are, however, based on some modelling assumptions, such as the unimodality of the response of the pollen taxa to climate (ter Braak and Juggins 1993). This condition is not always met at the continental scale, primarily because of the limited taxonomic resolution of pollen data that merges several plant species with distinct climate requirements as one single pollen taxon. WA-PLS_tailored has the same limitation but it has the advantage of reducing the influence of the correlation between variables when reconstructing, for instance, temperature and precipitation. This may be particularly relevant for regions with a temperature-moisture driven circulation system such as the East Asian Summer Monsoon (EASM) that can heavily affect precipitation patterns in certain regions (Herzschuh et al., 2019). Using WA-PLS_tailored also increases the number of records that pass a significance level of $p < 0.1$ (Telford and Birks, 2011). Providing several reconstructions based on different assumptions also allow exploring, even if only partially, the uncertainties associated with the modelling assumptions (e.g., MAT vs WA-PLS, the number of analogues, type metric used to compare pollen samples).

The significance tests sensu Telford and Birks (2011) revealed a rather low percentage of reconstructions to be substantial ($p < 0.1$). However, a failed significance test does not necessarily mean that the reconstruction is not reliable, but the results should be treated more cautiously, as the Telfold-Birks test is rather conservative (Luoto et al., 2014; Hébert et al., 2022). Several reasons of possible false negative errors are reported and discussed in the literature, including the test being supposed to be sensitive to the size of the training data, a low magnitude of an input climate signal, the trajectory of

536 the core samples through calibration space, or poor analog situations (Luoto et al., 2014; Self et al.,
537 2015; Andrén et al., 2015, Hébert et al., 2022).

538 All reconstruction methods used in this study heavily rely on extensive collections of modern
539 assemblage data covering diverse climatic and environmental gradients and are applicable on a broad
540 spatial scale. As discussed, all the methods may struggle with some intrinsic characteristics of pollen
541 data and of pollen compilations, including complex species responses, sensitivity to spatial
542 autocorrelation, limited analogues that may produce poor results in so-called “quantification deserts”
543 (Chevalier, 2019), where fossil pollen is hardly preserved or nearby modern surface pollen samples are
544 missing (Chevalier et al., 2020). However, we designed our datasets so that more methods can be
545 included in our reconstruction scripts (https://doi.org/10.5281/zenodo.5910989; Herzschuh et al.,
546 2022b), such as CREST, an approach that combines presence-only occurrence data from species
547 distribution databases instead of modern pollen samples to estimate the responses of pollen taxa to the
548 climate variable to reconstruct to a climate variable (Chevalier et al., 2014; Chevalier, 2022). CREST is,
549 therefore, more independent from the availability of modern pollen samples. Employing the Inverse-
550 Modelling through iterative forward modeling (IMIFM) (Izumi and Bartlein, 2016) might also be possible
551 in such regions. Its use would be particularly interesting to reconstruct the LGM samples, because
552 IMIFM is the only technique that can explicitly take the effect of CO_2 on plants (Chevalier et al., 2020).
553 The inclusion of CREST and/or IMIFM in such large-scale studies would complement our multi-model
554 reconstruction ensemble by exploring a larger fraction of the “method uncertainty” space in greater
555 details (e.g. Brewer et al, 2008). Kucera et al. (2005) propose several metrics for a multi-technique
556 approach to assess the uncertainty space: correlations between the residuals (observed minus
557 reconstructed values) between pairs of techniques are used to investigate the similarity in the
558 reconstructions among different techniques. The correlation between the residuals in seasonal
559 reconstructions (e.g. summer and winter temperatures, summer and annual temperatures) can be used
560 to investigate the degree of independence of different seasonal reconstructions. Error rate estimates
561 (RMSEP) determined by cross validation of the calibration data sets and the leaving-one-out method
562 can be used to compare the calibration of individual transfer function techniques, though it should be
563 considered that error estimates may vary with the choice of the cross-validation procedure (Kucera et
564 al., 2005).

565

5.4 Potential use of LegacyClimate 1.0

Our LegacyPollen 1.0 fossil pollen synthesis (Herzschuh et al., 2022c) contains records from all over the Northern Hemisphere extratropics. We used this synthesis to produce our LegacyClimate 1.0 reconstruction data set, which thus can be used to infer spatio-temporal patterns in climate reconstructions that are not only limited to a local or regional scale. Although several hemispheric or global reconstruction studies exist, they have been largely restricted to temperature or have included relatively few records (Marcott et al., 2013; Marsicek et al., 2018; Routson et al., 2019; Kaufman et al., 2020a and 2020b). Our dataset is therefore a valuable addition. It may be used in a multi-proxy approach, synthesizing marine and terrestrial records in order to assess temperature development during the Holocene and can help to highlight possible interdependencies between oceans and land masses. Globally or hemispherically averaged temperature reconstructions from proxy data indicate peak temperatures during the Holocene Thermal Maximum around 6000 years BP followed by a pronounced cooling trend toward the late Holocene, which is also visible in our pollen-based reconstructions (Fig. 10). Hence, spatial variability in the Holocene temperature trends (e.g. missing of a pronounced maximum for certain latitudinal bands; delayed thermal maximum on land compared to the ocean) indicate a more local rather than a global Holocene Thermal Maximum (Kaufman et al., 2020b; Osman et al., 2021; Cartapanis et al., 2022). In contrast, climate models simulate a monotonic warming throughout the Holocene, which resulted in the “Holocene conundrum” debate (Liu et al., 2014). The debate has since progressed and hints to discrepancies in data-model comparisons due to spatiotemporal dynamics related to heterogeneous responses to climate forcing and feedbacks (i.e. the timing of a Holocene Thermal Maximum in the Northern Hemisphere extra-tropics between reconstructions from continental and from marine proxy records; Cartapanis et al., 2022) and sometimes poor spatial averaging due to unevenly distributed proxies. Proxy-only reconstructions often rely on latitudinal binning and weighting, which makes this approach particularly sensitive to latitudinal bands that contain only sparse spatial coverage and thus do not represent a true global average (Osman et al., 2021). Those spatiotemporal dynamics should be considered in data-model comparison.

Temperature reconstructions often use either mean annual temperatures (Birks, 2019; Bova et al., 2021) or global mean surface temperatures (Marcott et al., 2013; Marsicek et al., 2018; Kaufman et al., 2020a and 2020b). Despite T_{ann} being more commonly used in multi-proxy comparisons, it might be useful to also consider T_{July}, as on a regional scale the mean July temperature (or in general summer temperature)

596 is more important in particular in high latitudes. However, it is argued that proxy-based climate
597 reconstructions are seasonally biased and therefore might be the reason for the observed proxy-model
598 divergence (Liu et al., 2014; Rehfeld et al., 2016; Kaufman et al., 2020b). In this respect, it might help
599 that we provide T_{July} along with T_{ann} reconstructions derived from our tailoring approach, which provides
600 the opportunity to assess seasonal impacts on the reconstruction (especially in the high latitudes) in
601 addition to a consistent reconstruction synthesis.

602 So far, reconstructions of precipitation have not been implemented on a hemispheric scale. The
603 interconnection between temperature and precipitation (Trenberth, 2011) and its spatio-temporal
604 variation across the Northern Hemisphere is therefore an important aspect of evaluating climate models
605 (Wu et al., 2013; Hao et al., 2019; Herzschuh et al., 2022a). A broad-scale quantitative reconstruction
606 of temperature and precipitation would therefore be of great value for evaluating transient climate model
607 experiments such as TraCE 21k (He, 2010).

608

609 **6 Data and code availability**

610 The compilation of reconstructed T_{July}, T_{ann}, and P_{ann}, is open access and available at PANGAEA
611 (https://doi.pangaea.de/10.1594/PANGAEA.930512; in the "*Other version*" section; Herzschuh et al.,
612 2021). The dataset files are stored in machine-readable data format (.CSV), which are already separated
613 into Western North America, Eastern North America, Europe, and Asia for easy access and use.

614 The R code to run the reconstructions for single sites is available at Zenodo
615 (https://doi.org/10.5281/zenodo.5910989; Herzschuh et al., 2022b) including harmonized open-access
616 modern and fossil pollen datasets so that customized reconstructions can be easily established.

617

618 **Author contributions.** UH designed the study design and reconstruction dataset. CL and TB compiled
619 the metadata and the harmonized pollen dataset. TB wrote the R scripts and ran the analyses under the
620 supervision of UH. UH, TB and MC wrote the first draft of the manuscript. All authors discussed the
621 results and contributed to the final manuscript.

Competing interests. The contact author has declared that none of the authors has any competing interests.

Acknowledgements. We would like to express our gratitude to all the palynologists and geologists who, either directly or indirectly by providing their work the Neotoma Paleoecology Database, contributed pollen data and chronologies to the dataset. The work of data contributors, data stewards, and the Neotoma community is gratefully acknowledged. We thank Andrej Andreev, Mareike Wieczorek, and Birgit Heim from AWI for providing information on pollen records and data uploads. We also thank Cathy Jenks for language editing on a previous version of the paper.

Financial support. This research has been supported by the European Research Council (ERC Glacial Legacy 772852 to UH) and the PalMod Initiative (01LP1510C to UH). TB and MC are supported by the German Federal Ministry of Education and Research (BMBF) as a Research for Sustainability initiative (FONA; https://www.fona.de/en) through the PalMod Phase II project (grant no. FKZ: 01LP1926D). CL holds a scholarship from the Chinese Scholarship Council (grant no. 201908130165). NR work was supported by the Russian Science Foundation (Grant No. 20-17-00110).

References

Andrén, E., Klimaschewski, A., Self, A. E., St. Amour, N., Andreev, A. A., Bennett, K. D., Conley, D. J., Edwards, T. W. D., Solovieva, N., and Hammarlund, D.: Holocene climate and environmental change in north-eastern Kamchatka (Russian Far East), inferred from a multi-proxy study of lake sediments, Global and Planetary Change, 134, 41–54, https://doi.org/10.1016/j.gloplacha.2015.02.013, 2015.

Behre, K. E.: The rôle of man in European vegetation history. In: Huntley, B., Webb, T. (eds) Vegetation history. Handbook of vegetation science, vol 7. Springer, Dordrecht. https://doi.org/10.1007/978-94-009-3081-0_17, 1988.

Birks, H. J. B.: Contributions of Quaternary botany to modern ecology and biogeography, Plant Ecol. Divers., 12, 189–385, https://doi.org/10.1080/17550874.2019.1646831, 2019.

Birks, H. J. B., Heiri, O., Seppä, H., and Bjune, A. E.: Strengths and Weaknesses of Quantitative Climate Reconstructions Based on Late-Quaternary, Open Ecol. J., 3, 68–110, http://dx.doi.org/10.2174/1874213001003020068, 2010.

Blaauw, M. and Christen, J. A.: Flexible paleoclimate age-depth models using an autoregressive gamma process, Bayesian Anal., 6, 457–474, https://doi.org/10.1214/11-BA618, 2011.

Blois, J. L., Williams, J. W., Grimm, E. C., Jackson, S. T., and Graham, R. W.: A methodological framework for assessing and reducing temporal uncertainty in paleovegetation mapping from late-Quaternary pollen records, Quat. Sci. Rev., 30, 1926–1939, https://doi.org/10.1016/j.quascirev.2011.04.017, 2011.

Bova, S., Rosenthal, Y., Liu, Z., Godad, S. P., and Yan, M.: Seasonal origin of the thermal maxima at the Holocene and the last interglacial, Nature, 589, 548–553, https://doi.org/10.1038/s41586-020-03155-x, 2021.

Brewer, S., Guiot, J., Sánchez-Goñi, M. F., and Klotz, S.: The climate in Europe during the Eemian: a multi-method approach using pollen data, Quaternary Science Reviews, 27, 2303–2315, https://doi.org/10.1016/j.quascirev.2008.08.029, 2008.

Cao, X., Ni, J., Herzschuh, U., Wang, Y., and Zhao, Y.: A late Quaternary pollen dataset from eastern continental Asia for vegetation and climate reconstructions: Set up and evaluation, Rev. Palaeobot. Palynol., 194, 21–37, https://doi.org/10.1016/j.revpalbo.2013.02.003, 2013.

Cao, X., Herzschuh, U., Telford, R. J., and Ni, J.: A modern pollen–climate dataset from China and Mongolia: Assessing its potential for climate reconstruction, Rev. Palaeobot. Palynol., 211, 87–96, https://doi.org/10.1016/j.revpalbo.2014.08.007, 2014.

Cao, X., Tian, F., Telford, R. J., Ni, J., Xu, Q., Chen, F., Liu, X., Stebich, M., Zhao, Y., Herzschuh, U.,: Impacts of the spatial extent of pollen-climate calibration-set on the absolute values, range and trends of reconstructed Holocene precipitation. Quaternary Science Reviews 178, 37-53. https://doi.org/10.1016/j.quascirev.2017.10.030, 2017.

Cao, X., Tian, F., Andreev, A., Anderson, P. M., Lozhkin, A. V., Bezrukova, E., Ni, J., Rudaya, N., Stobbe, A., Wieczorek, M., and Herzschuh, U.: A taxonomically harmonized and temporally

675 standardized fossil pollen dataset from Siberia covering the last 40 kyr, Earth Syst. Sci. Data, 12,
676 119–135, https://doi.org/10.5194/essd-12-119-2020, 2020.

677 Cartapanis, O., Jonkers, L., Moffa-Sanchez, P., Jaccard, S. L., and de Vernal, A.: Complex spatio-
678 temporal structure of the Holocene Thermal Maximum, Nat Commun, 13, 5662,
679 https://doi.org/10.1038/s41467-022-33362-1, 2022.

680 Chen, F., Chen, J., Huang, W., Chen, S., Huang, X., Jin, L., Jia, J., Zhang, X., An, C., Zhang, J., Zhao,
681 Y., Yu, Z., Zhang, R., Liu, J., Zhou, A., and Feng, S.: Westerlies Asia and monsoonal Asia:
682 Spatiotemporal differences in climate change and possible mechanisms on decadal to sub-orbital
683 timescales, Earth Sci. Rev., 192, 337–354, https://doi.org/10.1016/j.earscirev.2019.03.005, 2019.

684 Chevalier, M.: Enabling possibilities to quantify past climate from fossil assemblages at a global scale,
685 Glob. Planet. Change, 175, 27–35, https://doi.org/10.1016/j.gloplacha.2019.01.016, 2019.

686 Chevalier, M.: *crestr*: an R package to perform probabilistic climate reconstructions from
687 palaeoecological datasets, Clim. Past, 18, 821–844, https://doi.org/10.5194/cp-18-821-2022, 2022.

688 Chevalier, M., Cheddadi, R., and Chase, B. M.: CREST (Climate REconstruction SofTware): a
689 probability density function (PDF)-based quantitative climate reconstruction method, Clim. Past, 10,
690 2081–2098, https://doi.org/10.5194/cp-10-2081-2014, 2014.

691 Chevalier, M., Davis, B. A. S., Heiri, O., Seppä, H., Chase, B. M., Gajewski, K., Lacourse, T., Telford,
692 R. J., Finsinger, W., Guiot, J., Kühl, N., Maezumi, S. Y., Tipton, J. R., Carter, V. A., Brussel, T.,
693 Phelps, L. N., Dawson, A., Zanon, M., Vallé, F., Nolan, C., Mauri, A., de Vernal, A., Izumi, K.,
694 Holmström, L., Marsicek, J., Goring, S., Sommer, P. S., Chaput, M., and Kupriyanov, D.: Pollen-
695 based climate reconstruction techniques for late Quaternary studies, Earth Sci. Rev., 210, 103384,
696 https://doi.org/10.1016/j.earscirev.2020.103384, 2020.

697 Davis, B. A. S., Zanon, M., Collins, P., Mauri, A., Bakker, J., Barboni, D., Barthelmes, A., Beaudouin,
698 C., Bjune, A. E., Bozilova, E., Bradshaw, R. H. W., Brayshay, B. A., Brewer, S., Brugiapaglia, E.,
699 Bunting, J., Connor, S. E., de Beaulieu, J.-L., Edwards, K., Ejarque, A., Fall, P., Florenzano, A.,
700 Fyfe, R., Galop, D., Giardini, M., Giesecke, T., Grant, M. J., Guiot, J., Jahns, S., Jankovská, V.,
701 Juggins, S., Kahrmann, M., Karpińska-Kołaczek, M., Kołaczek, P., Kühl, N., Kuneš, P., Lapteva, E.

G., Leroy, S. A. G., Leydet, M., Guiot, J., Jahns, S., Jankovská, V., Juggins, S., Kahrmann, M., Karpińska-Kołaczek, M., Kołaczek, P., Kühl, N., Kuneš, P., Lapteva, E. G., Leroy, S. A. G., Leydet, M., López Sáez, J. A., Masi, A., Matthias, I., Mazier, F., Meltsov, V., Mercuri, A. M., Miras, Y., Mitchell, F. J. G., Morris, J. L., Naughton, F., Nielsen, A. B., Novenko, E., Odgaard, B., Ortu, E., Overballe-Petersen, M. V., Pardoe, H. S., Peglar, S. M., Pidek, I. A., Sadori, L., Seppä, H., Severova, E., Shaw, H., Święta-Musznicka, J., Theuerkauf, M., Tonkov, S., Veski, S., van der Knaap, W. O., van Leeuwen, J. F. N., Woodbridge, J., Zimny, M., and Kaplan, J. O.: The European Modern Pollen Database (EMPD) project, Veg. Hist. Archaeobot., 22, 521–530, https://doi.org/10.1007/s00334-012-0388-5, 2013.

Davis, B. A. S., Chevalier, M., Sommer, P., Carter, V. A., Finsinger, W., Mauri, A., Phelps, L. N., Zanon, M., Abegglen, R., Åkesson, C. M., Alba-Sánchez, F., Anderson, R. S., Antipina, T. G., Atanassova, J. R., Beer, R., Belyanina, N. I., Blyakharchuk, T. A., Borisova, O. K., Bozilova, E., Bukreeva, G., Bunting, M. J., Clò, E., Colombaroli, D., Combourieu-Nebout, N., Desprat, S., Di Rita, F., Djamali, M., Edwards, K. J., Fall, P. L., Feurdean, A., Fletcher, W., Florenzano, A., Furlanetto, G., Gaceur, E., Galimov, A. T., Gałka, M., García-Moreiras, I., Giesecke, T., Grindean, R., Guido, M. A., Gvozdeva, I. G., Herzschuh, U., Hjelle, K. L., Ivanov, S., Jahns, S., Jankovska, V., Jiménez-Moreno, G., Karpińska-Kołaczek, M., Kitaba, I., Kołaczek, P., Lapteva, E. G., Latałowa, M., Lebreton, V., Leroy, S., Leydet, M., Lopatina, D. A., López-Sáez, J. A., Lotter, A. F., Magri, D., Marinova, E., Matthias, I., Mavridou, A., Mercuri, A. M., Mesa-Fernández, J. M., Mikishin, Y. A., Milecka, K., Montanari, C., Morales-Molino, C., Mrotzek, A., Muñoz Sobrino, C., Naidina, O. D., Nakagawa, T., Nielsen, A. B., Novenko, E. Y., Panajiotidis, S., Panova, N. K., Papadopoulou, M., Pardoe, H. S., Pędziszewska, A., Petrenko, T. I., Ramos-Román, M. J., Ravazzi, C., Rösch, M., Ryabogina, N., Sabariego Ruiz, S., Salonen, J. S., Sapelko, T. V., Schofield, J. E., Seppä, H., Shumilovskikh, L., Stivrins, N., Stojakowits, P., Svobodova Svitavska, H., Święta-Musznicka, J., Tantau, I., Tinner, W., Tobolski, K., Tonkov, S., Tsakiridou, M., et al.: The Eurasian Modern Pollen Database (EMPD), version 2, Earth Syst. Sci. Data, 12, 2423–2445, https://doi.org/10.5194/essd-12-2423-2020, 2020.

Eyring, V., Cox, P. M., Flato, G. M., Gleckler, P. J., Abramowitz, G., Caldwell, P., Collins, W. D., Gier, B. K., Hall, A. D., Hoffman, F. M., Hurtt, G. C., Jahn, A., Jones, C. D., Klein, S. A., Krasting, J. P., Kwiatkowski, L., Lorenz, R., Maloney, E., Meehl, G. A., Pendergrass, A. G., Pincus, R., Ruane, A.

C., Russell, J. L., Sanderson, B. M., Santer, B. D., Sherwood, S. C., Simpson, I. R., Stouffer, R. J., and Williamson, M. S.: Taking climate model evaluation to the next level, Nat. Clim. Chang., 9, 102–110, https://doi.org/10.1038/s41558-018-0355-y, 2019.

Fick, S. E. and Hijmans, R. J.: WorldClim 2: new 1-km spatial resolution climate surfaces for global land areas, Int. J. Climatol., 37, 4302–4315, https://doi.org/10.1002/joc.5086, 2017.

Gajewski, K., Vance, R., Sawada, M., Fung, I., Gignac, L. D., Halsey, L., John, J., Maisongrande, P., Mandell, P., Mudie, P. J., Richard, P. J. H., Sherin, A. G., Soroko, J., and Vitt, D. H.: The climate of North America and adjacent ocean waters ca. 6 ka. Canadian Journal of Earth Sciences 37.5: 661-681, 2000.

Hao, Z., Phillips, T. J., Hao, F., and Wu, X.: Changes in the dependence between global precipitation and temperature from observations and model simulations, Int. J. Climatol., 39, 4895–4906, https://doi.org/10.1002/joc.6111, 2019.

He, F.: Simulating transient climate evolution of the last deglaciation with CCSM3, Ph.D. thesis, University of Wisconsin-Madison, USA, 185 pp., 2010.

Hébert, R., Herzschuh, U., and Laepple, T.: Millennial-scale climate variability over land overprinted by ocean temperature fluctuations, Nat. Geosci., 15, 899–905, https://doi.org/10.1038/s41561-022-01056-4, 2022.

Herzschuh, U., Cao, X., Laepple, T., Dallmeyer, A., Telford, R. J., Ni, J., Chen, F., Kong, Z., Liu, G., Liu, K.-B., Liu, X., Stebich, M., Tang, L., Tian, F., Wang, Y., Wischnewski, J., Xu, Q., Yan, S., Yang, Z., Yu, G., Zhang, Y., Zhao, Y., and Zheng, Z.: Position and orientation of the westerly jet determined Holocene rainfall patterns in China, Nat. Commun., 10, 2376, https://doi.org/10.1038/s41467-019-09866-8, 2019.

Herzschuh, U., Böhmer, T., Li, C., and Cao, X.: Northern Hemisphere temperature and precipitation reconstruction from taxonomically harmonized pollen data set with revised chronologies using WA-PLS and MAT (LegacyClimate 1.0), PANGAEA, https://doi.pangaea.de/10.1594/PANGAEA.930512, 2021.

758 Herzschuh, U., Böhmer, T., Li, C., Cao, X., Hébert, R., Dallmeyer, A., Telford, R. J., Kruse, S.:
759 Reversals in temperature-precipitation correlations in the Northern Hemisphere extratropics during
760 the Holocene. Geophysical Research Letters, p.e2022GL099730,
761 https://doi.org/10.1029/2022GL099730, 2022a.

762 Herzschuh, U., Böhmer, T., Li, C., Chevalier, M., Dallmeyer, A., Cao, X., Bigelow, N. H., Nazarova,
763 L., Novenko, E. Y., Park, J., Peyron, O., Rudaya, N. A., Schlütz, F., Shumilovskikh, L. S., Tarasov,
764 P. E., Wang, Y., Wen, R., Xu, Q., and Zheng, Z.: LegacyClimate 1.0: A dataset of pollen-based
765 climate reconstructions from 2594 Northern Hemisphere sites covering the late Quaternary [Data
766 set], Zenodo, https://doi.org/10.5281/zenodo.5910989, 2022b.

767 Herzschuh, U., Li, C., Böhmer, T., Postl, A. K., Heim, B., Andreev, A. A., Cao, X., Wieczorek, M., and
768 Ni, J.: LegacyPollen 1.0: a taxonomically harmonized global late Quaternary pollen dataset of 2831
769 records with standardized chronologies, Earth Syst. Sci. Data, 14, 3213–3227,
770 https://doi.org/10.5194/essd-14-3213-2022, 2022c.

771 Hijmans, R. J., van Etten, J., Sumner, M., Cheng, J., Baston, D., Bevan, A., Bivand, R., Busetto, L.,
772 Canty, M., Fasoli, B., Forrest, D., Ghosh, A., Golicher, D., Gray, J., Greenberg, J. A., Hiemstra, P.,
773 Hingee, K., Ilich, A., Institute for Mathematics Applied Geosciences, Karney, C., Mattiuzzi, M.,
774 Mosher, S., Naimi, B., Nowosad, J., Pebesma, E., Lamigueiro, O. P., Racine, E. B., Rowlingson,
775 B., Shortridge, A., Venables, B., and Wueest, R.: Raster: Geographic Data Analysis and Modeling,
776 R package version 3.5-11, https://cran.r-project.org/web/packages/raster, 2021.

777 Hill, M. O.: Diversity and Evenness: A Unifying Notation and Its Consequences, Ecology, 54, 427–
778 432, https://doi.org/10.2307/1934352, 1973.

779 Izumi, K. and Bartlein, P. J.: North American paleoclimate reconstructions for the Last Glacial
780 Maximum using an inverse modeling through iterative forward modeling approach applied to pollen
781 data: Pollen-Based Climate Reconstruction, Geophys. Res. Lett., 43, 10,965-10,972,
782 https://doi.org/10.1002/2016GL070152, 2016.

783 Jackson, S. T.: Pollen source area and representation in small lakes of the northeastern United States,
784 Rev. Palaeobot. Palynol., 63, 53–76, https://doi.org/10.1016/0034-6667(90)90006-5, 1990.

785 Jackson, S. T. and Williams, J. W.: MODERN ANALOGS IN QUATERNARY PALEOECOLOGY: Here
786 Today, Gone Yesterday, Gone Tomorrow?, Annu. Rev. Earth Planet. Sci., 32, 495–537,
787 https://doi.org/10.1146/annurev.earth.32.101802.120435, 2004.

788 Juggins, S.: Quantitative reconstructions in palaeolimnology: new paradigm or sick science?,
789 Quaternary Science Reviews, 64, 20–32, https://doi.org/10.1016/j.quascirev.2012.12.014, 2013.

790 Juggins, S.: rioja: Analysis of Quaternary Science Data, R package version 0.9-21, https://cran.r-
791 project.org/web/packages/rioja, 2019.

792 Kaufman, D., McKay, N., Routson, C., Erb, M., Davis, B., Heiri, O., Jaccard, S., Tierney, J., Dätwyler,
793 C., Axford, Y., Brussel, T., Cartapanis, O., Chase, B., Dawson, A., de Vernal, A., Engels, S.,
794 Jonkers, L., Marsicek, J., Moffa-Sánchez, P., Morrill, C., Orsi, A., Rehfeld, K., Saunders, K.,
795 Sommer, P. S., Thomas, E., Tonello, M., Tóth, M., Vachula, R., Andreev, A., Bertrand, S.,
796 Biskaborn, B., Bringué, M., Brooks, S., Caniupán, M., Chevalier, M., Cwynar, L., Emile-Geay, J.,
797 Fegyveresi, J., Feurdean, A., Finsinger, W., Fortin, M.-C., Foster, L., Fox, M., Gajewski, K.,
798 Grosjean, M., Hausmann, S., Heinrichs, M., Holmes, N., Ilyashuk, B., Ilyashuk, E., Juggins, S.,
799 Khider, D., Koinig, K., Langdon, P., Larocque-Tobler, I., Li, J., Lotter, A., Luoto, T., Mackay, A.,
800 Magyari, E., Malevich, S., Mark, B., Massaferro, J., Montade, V., Nazarova, L., Novenko, E., Pařil,
801 P., Pearson, E., Peros, M., Pienitz, R., Płóciennik, M., Porinchu, D., Potito, A., Rees, A.,
802 Reinemann, S., Roberts, S., Rolland, N., Salonen, S., Self, A., Seppä, H., Shala, S., St-Jacques,
803 J.-M., Stenni, B., Syrykh, L., Tarrats, P., Taylor, K., van den Bos, V., Velle, G., Wahl, E., Walker, I.,
804 Wilmshurst, J., Zhang, E., and Zhilich, S.: A global database of Holocene paleotemperature records,
805 Sci. Data, 7, 115, https://doi.org/10.1038/s41597-020-0445-3, 2020a.

806 Kaufman, D., McKay, N., Routson, C., Erb, M., Dätwyler, C., Sommer, P. S., Heiri, O., and Davis, B.:
807 Holocene global mean surface temperature, a multi-method reconstruction approach, Sci. Data, 7,
808 201, https://doi.org/10.1038/s41597-020-0445-3, 2020b.

809 Kucera, M., Weinelt, M., Kiefer, T., Pflaumann, U., Hayes, A., Weinelt, M., Chen, M.-T., Mix, A. C.,
810 Barrows, T. T., Cortijo, E., Duprat, J., Juggins, S., and Waelbroeck, C.: Reconstruction of sea-
811 surface temperatures from assemblages of planktonic foraminifera: multi-technique approach
812 based on geographically constrained calibration data sets and its application to glacial Atlantic and

Pacific Oceans, Quaternary Science Reviews, 24, 951–998, https://doi.org/10.1016/j.quascirev.2004.07.014, 2005.

Li, C., Postl, A. K., Böhmer, T., Cao, X., Dolman, A. M., and Herzschuh, U.: Harmonized chronologies of a global late Quaternary pollen dataset (LegacyAge 1.0), Earth Syst. Sci. Data, 14, 1331–1343, https://doi.org/10.5194/essd-14-1331-2022, 2022.

Liu, Z., Zhu, J., Rosenthal, Y., Zhang, X., Otto-Bliesner, B. L., Timmermann, A., Smith, R. S., Lohmann, G., Zheng, W., and Timm, O. E.: The Holocene temperature conundrum, PNAS, 111, E3501–E3505, https://doi.org/10.1073/pnas.1407229111, 2014.

Luoto, T. P., Kaukolehto, M., Weckström, J., Korhola, A., and Väliranta, M.: New evidence of warm early-Holocene summers in subarctic Finland based on an enhanced regional chironomid-based temperature calibration model, Quat. res., 81, 50–62, https://doi.org/10.1016/j.yqres.2013.09.010, 2014.

Marcott, S. A., Shakun, J. D., Clark, P. U., and Mix, A. C.: A Reconstruction of Regional and Global Temperature for the Past 11,300 Years, Science, 339, 1198–1201, https://doi.org/10.1126/science.1228026, 2013.

Marsicek, J., Shuman, B. N., Bartlein, P. J., Shafer, S. L., and Brewer, S.: Reconciling divergent trends and millennial variations in Holocene temperatures, Nature, 554, 92–96, https://doi.org/10.1038/nature25464, 2018.

Mauri, A., Davis, B. A. S., Collins, P. M., and Kaplan, J. O.: The climate of Europe during the Holocene: a gridded pollen-based reconstruction and its multi-proxy evaluation, Quat. Sci. Rev., 112, 109–127, https://doi.org/10.1016/j.quascirev.2015.01.013, 2015.

Nychka, D., Furrer, R., Paige, J., Sain, S., Gerber, F., and Iverson, M.: fields: Tools for Spatial Data, R package version 10.3, https://cran.r-project.org/web/packages/fields/index.html, 2020.

Oksanen, J., Blanchet, F. G., Friendly, M., Kindt, R., Legendre, P., McGlinn, D., Minchin, P. R., O'Hara, R. B., Simpson, G. L., Solymos, P., Stevens, M. H. H., Szoecs, E., and Wagner, H.: Vegan: Community Ecology Package, R package version 2.5-7, https://cran.r-project.org/web/packages/vegan, 2020.

Osman, M. B., Tierney, J. E., Zhu, J., Tardif, R., Hakim, G. J., King, J., and Poulsen, C. J.: Globally resolved surface temperatures since the Last Glacial Maximum, Nature, 599, 239–244, https://doi.org/10.1038/s41586-021-03984-4, 2021.

Overpeck, J. T., Webb, T., and Prentice, I. C.: Quantitative Interpretation of Fossil Pollen Spectra: Dissimilarity Coefficients and the Method of Modern Analogs, Quat. Res., 23, 87–108, https://doi.org/10.1016/0033-5894(85)90074-2, 1985.

Parnell, A. C., Haslett, J., Sweeney, J., Doan, T. K., Allen, J. R. M., and Huntley, B.: Joint palaeoclimate reconstruction from pollen data via forward models and climate histories, Quaternary Science Reviews, 151, 111–126, https://doi.org/10.1016/j.quascirev.2016.09.007, 2016.

R Core Team: R: A language and environment for statistical computing, R Foundation for Statistical Computing, Vienna, Austria, available online at: https://www.R-project.org/, 2020.

Rehfeld, K., Trachsel, M., Telford, R. J., and Laepple, T.: Assessing performance and seasonal bias of pollen-based climate reconstructions in a perfect model world, Clim. Past, 12, 2255–2270, https://doi.org/10.5194/cp-12-2255-2016, 2016.

Routson, C. C., McKay, N. P., Kaufman, D. S., Erb, M. P., Goosse, H., Shuman, B. N., Rodysill, J. R., and Ault, T.: Mid-latitude net precipitation decreased with Arctic warming during the Holocene, Nature, 568, 83–87, https://doi.org/10.1038/s41586-019-1060-3, 2019.

Self, A. E., Jones, V. J., and Brooks, S. J.: Late Holocene environmental change in arctic western Siberia, The Holocene, 25, 150–165, https://doi.org/10.1177/0959683614556387, 2015.

Simpson, G. L.: Analogue Methods in Palaeolimnology, in: Tracking Environmental Change Using Lake Sediments: Data Handling and Numerical Techniques, edited by: Birks, H. J. B., Lotter, A. F., Juggins, S., and Smol, J. P., Springer Netherlands, Dordrecht, 495–522, https://doi.org/10.1007/978-94-007-2745-8_15, 2012.

Simpson, G. L., Oksanen, J., Maechler, M.: analogue: Analogue and Weighted Averaging Methods for Palaeoecology, R package version 0.17-6, https://cran.r-project.org/web/packages/analogue, 2021.

Sugita, S.: A Model of Pollen Source Area for an Entire Lake Surface, Quat. Res., 39, 239–244, https://doi.org/10.1006/qres.1993.1027, 1993.

Tarasov, P. E., Nakagawa, T., Demske, D., Österle, H., Igarashi, Y., Kitagawa, J., Mokhova, L., Bazarova, V., Okuda, M., Gotanda, K., Miyoshi, N., Fujiki, T., Takemura, K., Yonenobu, H., and Fleck, A.: Progress in the reconstruction of Quaternary climate dynamics in the Northwest Pacific: A new modern analogue reference dataset and its application to the 430-kyr pollen record from Lake Biwa, Earth Sci. Rev., 108, 64–79, https://doi.org/10.1016/j.earscirev.2011.06.002, 2011.

Telford, R. J.: palaeoSig: Significance Tests for Palaeoenvironmental Reconstructions, R package version 2.0-3, https://cran.r-project.org/web/packages/palaeoSig, 2019.

Telford, R. J. and Birks, H. J. B.: A novel method for assessing the statistical significance of quantitative reconstructions inferred from biotic assemblages, Quat. Sci. Rev., 30, 1272–1278, https://doi.org/10.1016/j.quascirev.2011.03.002, 2011.

ter Braak, C. J. F.: CANOCO - a FORTRAN program for canonical community ordination by (Partial) (Detrended) (Canonical) correspondence analysis and redundancy analysis. Agricultural Mathematics Group, Wageningen, 1988.

ter Braak, C. J. F. and Juggins, S.: Weighted averaging partial least squares regression (WA-PLS): an improved method for reconstructing environmental variables from species assemblages, Hydrobiologia, 269, 485–502, https://doi.org/10.1007/BF00028046, 1993.

Tian, F., Cao, X., Dallmeyer, A., Zhao, Y., Ni, J., and Herzschuh, U.: Pollen-climate relationships in time (9 ka, 6 ka, 0 ka) and space (upland vs. lowland) in eastern continental Asia, Quat. Sci. Rev., 156, 1–11, https://doi.org/10.1016/j.quascirev.2016.11.027, 2017.

Trachsel, M. and Telford, R. J.: All age–depth models are wrong, but are getting better, Holocene, 27, 860–869, https://doi.org/10.1177/0959683616675939, 2017.

Trenberth, K. E.: Changes in precipitation with climate change, Clim. Res., 47, 123–138, https://doi.org/10.3354/cr00953, 2011.

Whitmore, J., Gajewski, K., Sawada, M., Williams, J. W., Shuman, B., Bartlein, P. J., Minckley, T., Viau, A. E., Webb, T., Shafer, S., Anderson, P., and Brubaker, L.: Modern pollen data from North America and Greenland for multi-scale paleoenvironmental applications, Quat. Sci. Rev., 24, 1828–1848, https://doi.org/10.1016/j.quascirev.2005.03.005, 2005.

Williams, J. W., Grimm, E. C., Blois, J. L., Charles, D. F., Davis, E. B., Goring, S. J., Graham, R. W., Smith, A. J., Anderson, M., Arroyo-Cabrales, J., Ashworth, A. C., Betancourt, J. L., Bills, B. W., Booth, R. K., Buckland, P. I., Curry, B. B., Giesecke, T., Jackson, S. T., Latorre, C., Nichols, J., Purdum, T., Roth, R. E., Stryker, M., and Takahara, H.: The Neotoma Paleoecology Database, a multiproxy, international, community-curated data resource, Quat. Res., 89, 156–177, https://doi.org/10.1017/qua.2017.105, 2018.

Williams, J. W., Webb III, T., Richard, P. H., and Newby, P.: Late Quaternary biomes of Canada and the eastern United States, J. Biogeogr., 27, 585–607, https://doi.org/10.1046/j.1365-2699.2000.00428.x, 2000.

Wu, R., Chen, J., and Wen, Z.: Precipitation-surface temperature relationship in the IPCC CMIP5 models, Adv. Atmos. Sci., 30, 766–778, https://doi.org/10.1007/s00376-012-2130-8, 2013.

Zanon, M., Davis, B. A. S., Marquer, L., Brewer, S., and Kaplan, J. O.: European Forest Cover During the Past 12,000 Years: A Palynological Reconstruction Based on Modern Analogs and Remote Sensing, Front. Plant Sci., 9, 253, https://doi.org/10.3389/fpls.2018.00253, 2018.

Appendix Figures

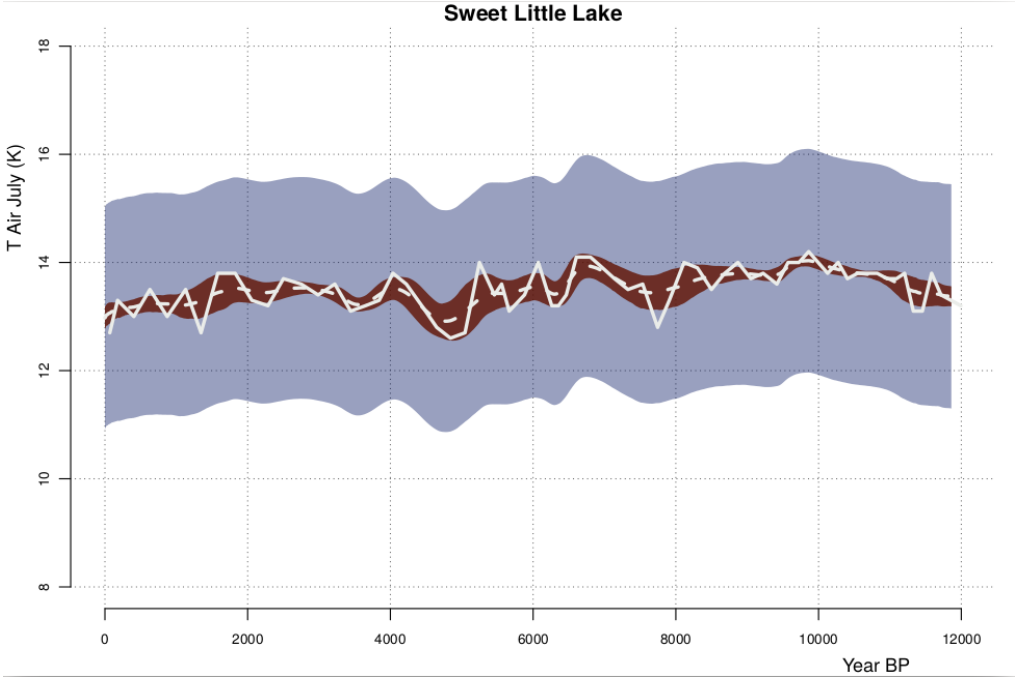

Appendix Figure 1. Reconstruction error (shaded blue) and the chronological error (shaded red) around the reconstruction smoothed by the time-uncertainty (i.e. when we interpolate at regular timesteps for the 1000 realizations and average over the ensemble, dashed white). The original reconstruction with the median ages is also shown for comparison (solid white); this underlines that averaging over the age models only preserves the low-frequencies but (unrealistically) smooths out the high-frequencies.

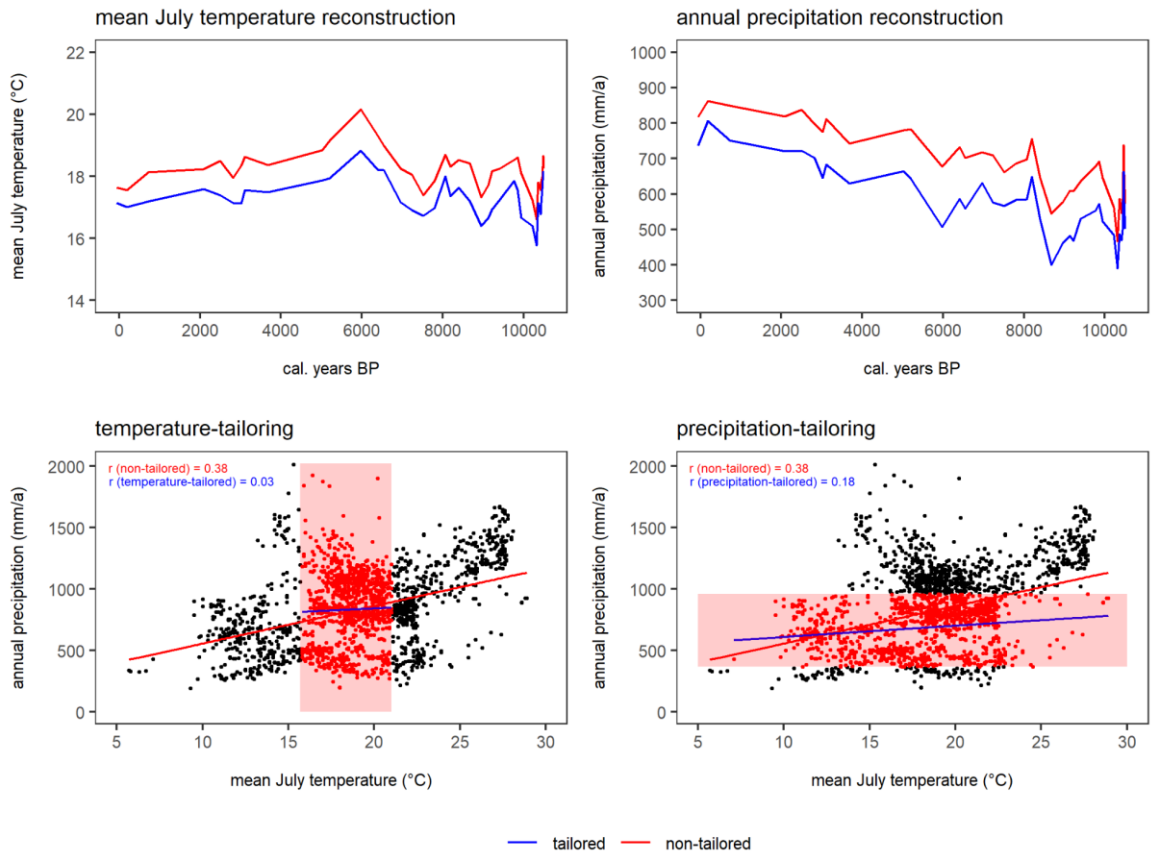

928

929 **Appendix Figure 2.** Example to illustrate the effect of tailoring the modern dataset for the location
930 "Yellow Dog Pond" in Eastern North America. Upper part: reconstruction of T_{July} and P_{ann} with WA-PLS
931 (red) and WA-PLS_tailored (blue); lower part: correlation of T_{July} and P_{ann} in the modern dataset and the
932 effect of tailoring the modern dataset (indicated with the red box). Correlations are given for non-tailored
933 (red) and tailored (blue) data.